Design parameters for injectable biopolymeric hydrogels with dynamic covalent chemistry crosslinks

Narelli de Paiva Narciso[1,a], Renato S. Navarro[1, a], Aidan Gilchrist[1], Miriam L. M. Trigo[1], Giselle Aviles Rodriguez[1], Sarah C. Heilshorn[1,*]

1 Department of Materials Science and Engineering, Stanford University, Stanford, CA 94305, USA.

[a] These two authors contributed equally to this work.

* Person to whom correspondence should be addressed, heilshorn@stanford.edu

ABSTRACT

Dynamic covalent chemistry (**DCC**) crosslinks can form hydrogels with tunable mechanical properties permissive to injectability and self-healing. However, not all hydrogels with transient crosslinks are easily extrudable. For this reason, two additional design parameters must be considered when formulating DCC-crosslinked hydrogels: 1) degree of functionalization (**DoF**) and 2) polymer molecular weight (**MW**). To investigate these parameters, we formulated hydrogels comprised of two recombinant biopolymers: (1) a hyaluronic acid (**HA**) modified with benzaldehyde (**HA-BZA**) and (2) an elastin-like protein (**ELP**) modified with hydrazine (**ELP-HYD**). We synthesized several hydrogel families with distinct HA MW and DoF while keeping the ELP-HYD component constant. The resulting hydrogels had a range of stiffnesses, $G' \sim$ 10-1000 Pa, and extrudability, which was attributed to the combined effects of DCC crosslinks and polymer entanglements. In general, lower MW formulations required lower forces for injectability, regardless of stiffness. Higher DoF formulations exhibited more rapid self-healing. Gel extrusion through a cannula (2-m length, 0.25-mm diameter) demonstrated the potential for minimally-invasive delivery for future biomedical applications. In summary, this work highlights additional parameters that influence the injectability and network formation of DCC-crosslinked hydrogels and aims to guide future design of injectable hydrogels.

1. Introduction

Hydrogels have extensive biomedical applications, including tissue engineering, medical devices, and therapeutic delivery vehicles.[1] One of the key benefits of hydrogels is the tunable range of their mechanical properties (e.g., stiffness, self-healing, and remodeling) that allows them to replicate essential features of the natural extracellular matrix (**ECM**).[2-4] Furthermore, the potential extrudability of hydrogels is beneficial for clinical translation,[5] as injection is a favorable route for delivery of cells and

pharmaceuticals, including proteins[6-8] and gene therapies.[9-11] However, producing hydrogels that are simultaneously injectable, encompass a broad range of stiffness, and retain their mechanical properties post-extrusion remains a challenge in the field. Physical gels depend on transient crosslinks, such as hydrogen bonds and van der Waals forces,[12] which generally allow for extrusion and injection. Nonetheless, the weak nature of these bonds results in low stiffness gels.[12,13] On the other hand, chemical gels depend on permanent crosslinks, which often provide increased stability and higher stiffness.[12,13] However, typically these permanent crosslinks prevent extrusion, requiring complex injection protocols,[13-15] which greatly limits their clinical translatability.

Dynamic covalent chemistry (**DCC**) has emerged as an alternative approach for hydrogel crosslinking.[16-19] The covalent nature of DCC provides mechanical strength to the hydrogel, while the transient behavior allows the polymer chains to associate and dissociate. This can enable injectability and recovery of the polymer network post-extrusion, regaining the original mechanical properties.[17,20] However, not all DCC hydrogels are injectable,[21] especially using only hand-force as the extrusion method, and not all DCC hydrogels are able to fully recover their pre-injection mechanical properties.[22-25] Literature has shown that properties at both the single macromolecule level (e.g., polymer molecular weight)[26-28] and the network level (e.g., density of crosslinks) can directly affect the extrudability of gels.[29-31] Thus, while DCC crosslinking is often permissive for injectability, it is insufficient to universally predict hydrogel injection.

Using DCC strategies, our group has previously demonstrated extrusion of recombinant biomacromolecular hydrogels. Combining a chemically modified hyaluronic acid (HA), a linear polysaccharide, with a modified elastin-like protein (ELP), we created a highly tunable bioengineered hydrogel system, termed HELP.[21,32-35] HA is present throughout the native ECM, readily biodegradable, and easily functionalized for a variety of

crosslinking schemes making it an ideal candidate for hydrogel synthesis.[15,19,36-38] Further, the design of ELP's amino acid sequence simultaneously confers mechanical elasticity (inclusion of repetitive elastin-like peptides), cell-adhesion (inclusion of fibronectin-derived RGD peptides), and facile chemical functionalization (inclusion of lysine residues with primary amine side chains) (**Fig. S1**).[39] Using an aldehyde-functionalized HA and a hydrazine-functionalized ELP, the resulting HELP hydrogel is stabilized through hydrazone bonds, a dynamic covalent crosslink (**Fig. 1A-C**). Previous work demonstrated that these HELP hydrogels support the culture of primary human adult intestinal organoids,[34] can deliver therapeutics to the myocardium[40,41] and can be formulated as a bioink for 3D printing.[35] Furthermore, the system's stiffness is tunable through several variables, including crosslinking temperature, degree of chemical functionalization, and polymer concentration.[32] In addition, HELP formulations have been shown to increase payload retention in a demanding myocardial injection model, improving their clinical translation potential.[21,40] However, similar to other DCC hydrogels, predicting the hand-injectability of different HELP formulations is a challenge,[21] highlighting the lack of knowledge of the impact of hydrogel design parameters on injectability for DCC-crosslinked systems.

The versatility and synthetic control of the HA and ELP biopolymers make the HELP hydrogel system an ideal platform to address this fundamental knowledge gap. In this work, we evaluated the role of two macromolecular parameters, degree of functionalization and polymer molecular weight, in modulating injectability and recovery of mechanical properties for DCC-crosslinked HELP hydrogels. Specifically, we synthesized a family of HELP formulations, with identical ELP content and varying 1) HA degree of functionalization, with 6-30% of the carboxylic acids in the HA backbone modified to present benzaldehyde motifs, and 2) HA molecular weight between 20-500 kDa (**Fig. 1D**). Interestingly, while high molecular weight HA (1000 kDa or larger) is present in the healthy, native ECM, most HA used in engineered biomaterials have

molecular weights ranging from 100 – 250 kDa.[42-47] For hydrogels, the mechanical stiffness is related to the density of crosslinks, which can occur both through chemical crosslinking reactions as well as physical associations and entanglements.[20,48-52] We rationalized that both of our experimental variables were likely to alter the final hydrogel stiffness. Changing the degree of HA functionalization will alter the stoichiometric ratio of hydrazine to benzaldehyde reactive groups, and hence impact the density of chemical crosslinking sites within the gel network. We hypothesize that changing the HA molecular weight will lead to greater physical entanglements within the gel network. While the role of these parameters in controlling gel stiffness is somewhat intuitive, how they may impact injectability is less predictable, as injectability can be related to hydrogel stiffness[29-31] in addition to viscosity,[31] yield stress,[53-55] and fracture stress.[21] Furthermore, the ability of a material to regain its stiffness after injection is also challenging to predict. Thus, through systematic rheological analysis of this family of HELP hydrogels, we sought to relate these molecular-level design parameters to the final hydrogel stiffness, injectability, and ability to self-heal following extrusion. In particular, to demonstrate the potential for clinical translatability, we developed an *in vitro* model of catheter injection using a long, thin cannula (**Fig.1E**). As HA becomes an increasingly common component of engineered biomaterials, evaluating the relationship between HA molecular-level design parameters and final hydrogel material properties will become ever more important.

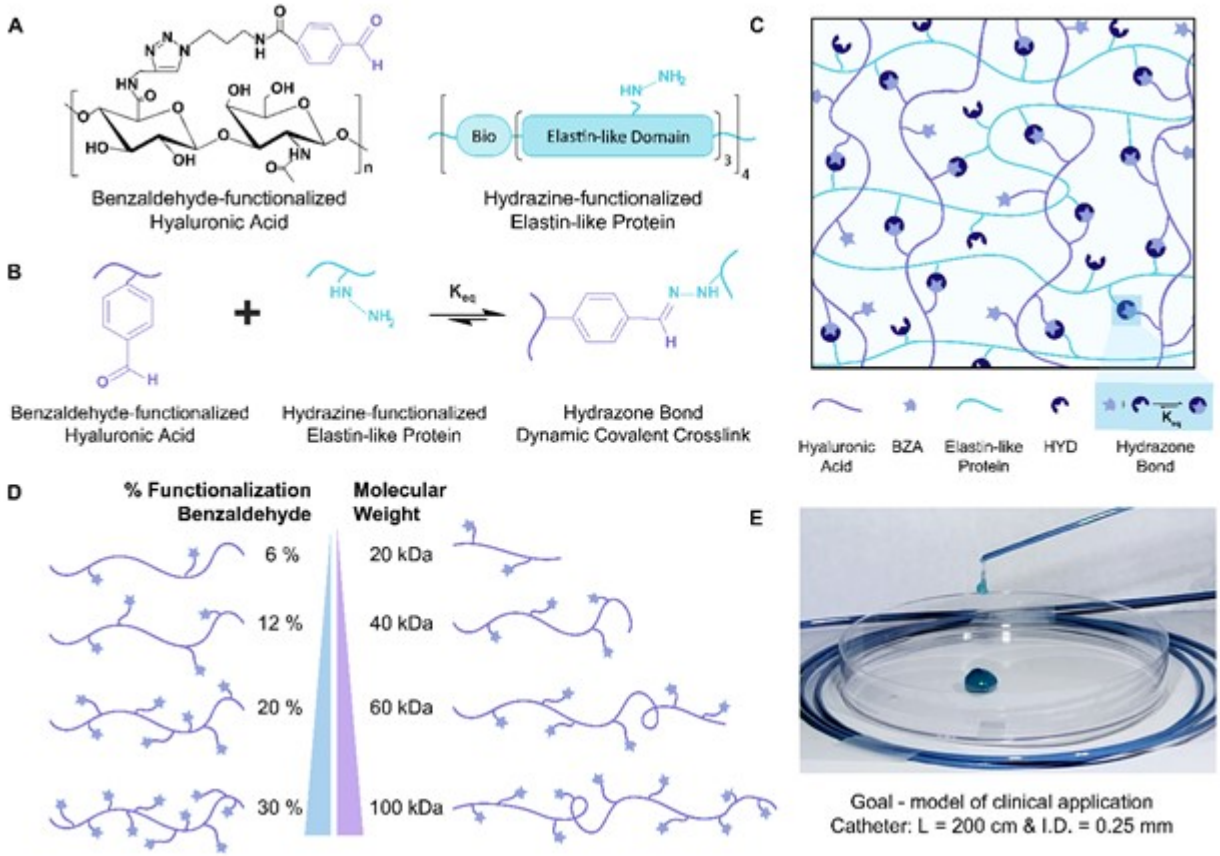

Figure 1. A. Chemical structure of hyaluronic acid (HA) modified with benzaldehyde (BZA) moiety, and scheme of elastin-like protein (ELP) modified with hydrazine (HYD) moiety. **B.** Representation of HA-BZA mixed with ELP-HYD, spontaneously forming a hydrazone bond, a dynamic covalent crosslink. **C.** Schematic of hydrogel network formed upon mixing, termed HELP gel. **D.** Schematic of variables in this study: percent modification of HA-BZA and molecular weight of HA. **E.** Model of injection through cannula (L = 200 cm, ID = 0.25 mm) to demonstrate our goal and clinical translatability

2. Results and Discussion

Click-chemistry allows for controlled functionalization of HA while maintaining polymer molecular weight

The recombinant ELP was synthesized by bacterial expression and purified by inverse temperature cycling as previously reported.[39] To modify the ELP with hydrazine groups, we performed an amidation of hydrazinoacetic acid onto the 14 lysine residues within the primary ELP amino acid sequence, resulting in ELP-HYD[32] (**Fig.1A, Fig. S2**). This same ELP component was used throughout all HELP formulations at a final concentration of 1 wt%.

Recombinant HA of varying molecular weights were purchased and bioconjugated with benzaldehyde (BZA) through the amidation of propargyl amine followed by a copper mediated click-chemistry reaction to synthesize HA-BZA,[34,56,57] (**Fig. S3**). Compared to oxidation, which is an alternative method to synthesize aldehyde-presenting HA, this click-chemistry approach does not result in polymer cleavage;[58,59] thus, this synthetic strategy retains the HA polymer molecular weight.[21,58-60] The degree of functionalization was tuned between 6-30% by varying the degree of amidation, and the final amount of benzaldehyde modification was confirmed by NMR (**Fig. S4-S8**). When mixed in a 1:1 ratio (by mass, final concentration of 1% wt ELP-HYD and 1 wt% HA-BZA) of ELP-HYD to HA-BZA, a gel is rapidly formed through the formation of hydrazone bonds that crosslink the two biopolymers together (**Fig.1B**). The benzaldehyde-hydrazine reaction has a relatively high equilibrium constant (K_{eq}),[61] which, results in stable HELP gels.[35] While the high BZA-HYD K_{eq} results in slower remodeling,[21] the crosslink still maintains its dynamic nature at physiological pH and temperature,[61] providing shear-thinning properties that may allow for hydrogel injectability.

While it has been hypothesized that the reversible nature of DCCs would invariably lead to injectable hydrogels,[13,16-18] that is not always the case. DCC hydrogels present a range of extrudability behavior, with many gel strategies that are too difficult to extrude by hand[21,35,62,63] or extrude as fragmented gels that cannot regain their original mechanical

properties.[35,64-68] Therefore, further exploration is necessary to uncover the fundamental design rules of dynamic polymer networks that would lead to hydrogels with both ease of injectability and robust mechanics. To probe our hypothesis that HA functionality and molecular weight would impact the injectability and final mechanical performance of the hydrogel, we first mechanically characterized the initial gel properties, including gelation time, stiffness, viscosity, and fracture stress.

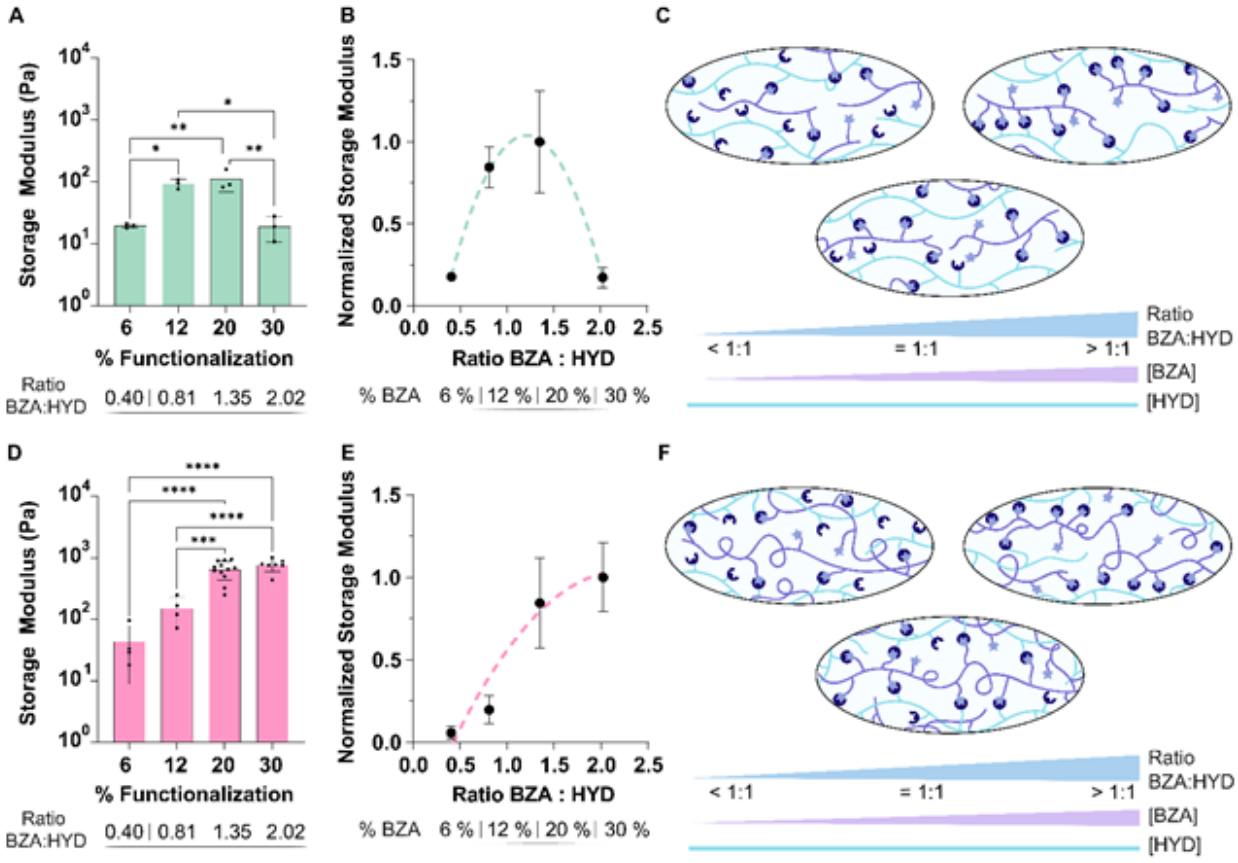

Figure 2. Gelation characterization of a family of HELP gels with 20-kDa and 40-kDa HA. A. Storage modulus of HELP formulations with 20-kDa HA with degree of BZA modification ranging from 6 to 30 %. **B.** Visualization of trend-lines of storage moduli

with respect to stoichiometric ratio of the crosslinking benzaldehyde to hydrazine functional groups (BZA:HYD) for HELP formulations with 20-kDa HA, with standard deviation (SD). SD values are listed in **Table S1**. **C.** Schematic of idealized mesoscale structure of HA and ELP biopolymers at varying BZA:HYD ratios for formulations with 20-kDa HA. **D.** Storage modulus of HELP formulations with 40-kDa HA. **E.** Storage moduli trend with respect to stoichiometric ratio of BZA:HYD with 40-kDa HA, with standard deviation. SD values are listed in **Table S1**. **F.** Schematic of idealized mesoscale structure at varying BZA:HYD ratios with 40-kDa HA. One-way ANOVA, *p < 0.05, **p< 0.01, ***p < 0.001, ****p < 0.0001.

At low HA molecular weights, degree of functionalization has a parabolic effect on gel stiffness

We combined the HA and ELP functionalized biopolymers to create a library of 15 HELP formulations, all of which had 1% HA-BZA and 1% ELP-HYD by weight in 10X isotonic phosphate-buffered saline (iPBS). Due to the pH sensitivity of the hydrazone reaction,[69] we selected to solubilize each biopolymer in 10X iPBS to provide stable buffering as the reaction proceeds. Each gel was mechanically characterized through rheological measurements assessing gelation time and storage (G') and loss (G'') moduli. These studies aimed to mirror the potential translational application, by mixing of the two components at room temperature (23 °C, 15 minutes) to assess gelation time, followed by an increase to 37 °C to simulate body temperature to assess initial gel stiffness. When injected *in vivo*, we would expect the ions in the 10X iPBS buffer to rapidly diffuse into the surrounding tissue and equilibrate with the surrounding fluid medium. Depending on the site of injection, this may alter the final *in situ* mechanical properties of the gel, as different body locations have different pH and ionic strengths.[70] In previous studies, we observed that measurement of initial gel stiffness *ex vivo* correlated with gel retention in the rat myocardium,[21] suggesting that relative mechanical properties measured *ex vivo* reflect relative properties *in vivo*.

The benzaldehyde-hydrazine reaction, responsible for the network crosslinking, has a stoichiometry of one BZA to one HYD moiety.[32,61,65] Thus, by varying the degree of BZA functionalization on the HA, we are directly changing the stoichiometric ratio of BZA to HYD functional groups (BZA:HYD), which will impact the crosslink formation and initial hydrogel stiffness.[12,71-73] We first evaluated the hydrogel gelation time, which we defined as the time required to reach a tan δ = G''/G' = 1, at 1 rad/s, 1% strain, and room temperature.[74-77] Even though gelation time measurements had large standard deviations, due to variations in mixing and start of data collection, there was a noticeable decrease in gelation time with an increase in BZA functionalization for all molecular weights (**Fig. S9)**. This trend indicates that the polymer network was formed more quickly as we increased the concentration of BZA in all HELP formulations, likely due to a combination of increased DCC reaction kinetics as the concentration of BZA reactant is increased[16] resulting in a crosslinking density that reaches the percolation threshold at earlier times.[12]

As previously reported, all HELP formulations experienced an increase in storage modulus (~200 Pa) as the temperature increased from 23 °C to 37 °C,[32] (**Fig. S10**). This stiffening effect is a consequence of the conformational change in the ELP component above its lower critical transition temperature ($\mathbf{T_t}$).[21,32,78] ELP forms protein-rich coacervates above the T_t, which serve as additional physical crosslinking sites[79] within the HELP formulations.[21,32] All gel formulations were held at 37 °C for 15 minutes to allow this process to occur prior to measurement of initial gel moduli.

In HELP formulations with the smallest HA (20 kDa), the gel stiffness followed a parabolic trend with respect to the ratio of BZA to HYD (BZA:HYD) (**Fig 2A-B**). Within this subfamily of gels (20 kDa HA), the maximum stiffness was achieved at a BZA:HYD

ratio close to 1:1, a behavior similar to that for chemical hydrogels crosslinked with static covalent bonds.[12,80,81] This parabolic behavior can be explained by examining the functional group ratio (BZA:HYD) to predict the total number of possible crosslinks between the biopolymers, (**Fig. 2B**). At ratios lower than 1:1, there is an excess of HYD moieties and not enough BZA available to react with each HYD (**Fig. 2C**). This results in a lower density of crosslinks and a lower storage modulus (average storage modulus (G'_{avg}) for gels with 6 % BZA was 19.7 $\pm$ 1.5 Pa).[12,71,73] At a 1:1 ratio of BZA:HYD, the actual concentration of available functional groups is similar to the stoichiometric ratio of the crosslinking reaction. Thus, all functional groups could potentially participate in crosslinking, which leads to an increased density of crosslinks and a higher storage modulus of approximately 100 Pa (G'_{avg} = 94.0 $\pm$ 16.8 Pa and G'_{avg} = 111.3 Pa $\pm$ 42.2, at 12% and 20% BZA respectively). As the concentration of BZA moieties to HYD moieties is further increased, there is now an excess of BZA moieties, leading to rapid formation of the network as evidenced by the decreased gelation time (**Fig. S9**). This rapid gelation leads to a high prevalence of gel defects, such as dangling bonds and loops, that do not structurally contribute to the continuous polymer network.[72,82-85] Further, as the HA biopolymer is relatively short (20 kDa, about half the length of the 37-kDa ELP), shorter percolating paths and fewer entanglements can be formed,[51,52,86-90] as the chains are unable to span across multiple neighboring ELP chains. These limitations decrease the effective density of crosslinks in the hydrogel, lowering the modulus (G'_{avg} = 19.2 $\pm$ 8.5 Pa at 30 % BZA).

For intermediate HA molecular weight, increasing the degree of functionalization will increase the gel stiffness

While the stiffness of HELP formulations with the 20-kDa HA follow a parabolic trend, HELP formulations with higher molecular weight (e.g. 40 kDa HA) presented an overall increase in stiffness as the BZA:HYD ratio increases (**Fig. 2D,E)**. Many theories, such as the sticky Rouse and the sticky reptation models[91-94] have been proposed to describe

the behavior of dynamically crosslinked hydrogels; however, Cai *et. al.* has recently developed a theoretical framework that considers the dynamic nature of the network on a self-consistent, single-chain level.[95,96] We rationalized that by considering the single-chain level, we could elucidate the effect of HA molecular weight on the stiffness of each subfamily. Termed Brachiation theory, this model describes the transitory union of the dynamic bonds along the chain backbone, allowing for a chain to move through the polymer network via a mechanism of transient reaching, grabbing, and releasing of other polymer chains.[95] An essential aspect of this theory is its consideration of the probability (pb) of the chain being bound at any moment, such that at equilibrium $pb = \frac{K_{eq} \times c \times M}{(1+K_{eq} \times c \times M)}$, where K_{eq} is the equilibrium constant, c the polymer-chain concentration, and M is the number of binding sites per chain.[95] Through this lens, HA chains with a higher number of BZA reactive sites will have a greater probability for more bound associations at any moment, contributing to a longer continuous percolating pathway throughout the network (**Fig. 2F**) and a stiffer gel.[86-90,95]

At BZA:HYD ratios smaller than 1:1, there are not enough BZA moieties to react with all HYD moieties, leading to low crosslink density and lower modulus[12] (40-kDa HA, 6 % BZA G'_{avg} = 44.0 $\pm$ 35.2 Pa). As the BZA:HYD ratio increases, the number of functional groups per HA chain is also increased, leading to an increase in modulus (40-kDa HA, G'_{avg} = 152.1 $\pm$ 75.3 Pa at 12% BZA; G'_{avg} = 652.5 $\pm$ 220.6 Pa at 20% BZA; and G'_{avg} = 773.3 $\pm$ 174.2 Pa at 30% BZA).

Thus, while the gel sub-family formulated with 20-kDa HA had a stiffer modulus near a BZA:HYD ratio of 1:1, for the 40-kDa HA sub-family the stiffest formulations occurred at higher BZA:HYD ratios, consistent with the prediction of Brachiation theory. The longer chain lengths of the 40-kDa HA sub-family have a greater likelihood to span across neighboring ELP chains (**Fig. 2F**), allowing for longer continuous paths through the

network.[12,86-90,95] In addition, the longer HA chains may enable the formation of entanglements that can also serve as effective structural crosslinks[92].

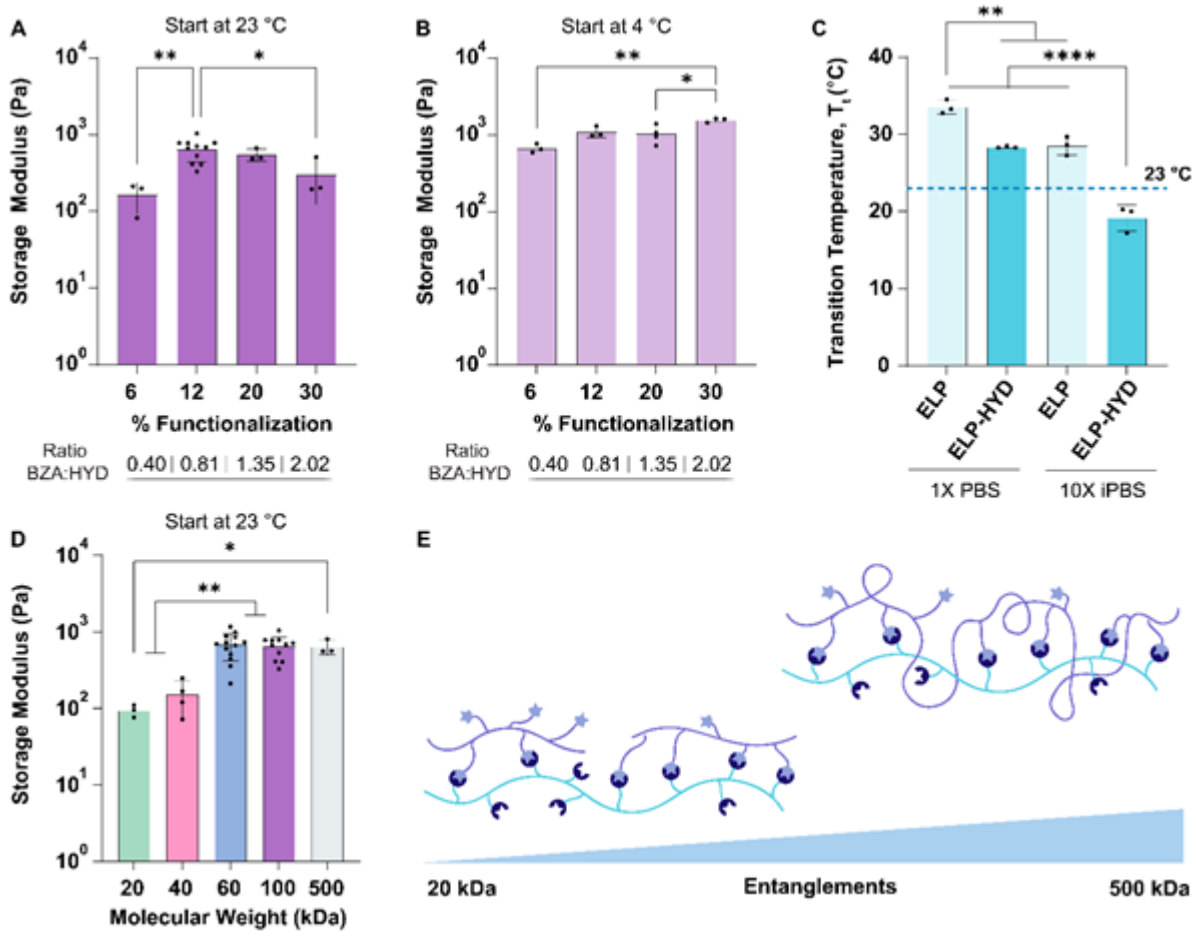

Figure 3. Effect of chain length on the stiffness of HELP gels. A & B. Storage moduli of HELP formulations with 100-kDa HA crosslinked at 23 °C (**A**), and 4 °C (**B**) with degree of BZA modification ranging from 6, 12, 20 and 30 %. **C.** Lower critical transition temperature (T_t) of ELP and ELP-HYD in 1X PBS and 10X isotonic PBS (10X iPBS), showing the temperature at which the polymer undergoes a conformational change. Chemical conjugation decreases the T_t, while 1X PBS increases solubility. **D**. Storage

moduli of all HELP formulations with 12 % BZA functionalization, with HA molecular weight ranging from 20 to 500 kDa crosslinked at 23 °C. **E.** Schematic of entanglements effects on storage moduli at increasing HA molecular weight. All data are averages +/- standard deviation, one-way ANOVA, *p < 0.05, **p< 0.01, ***p < 0.001, ****p < 0.0001.

Impact of chain entanglements and lower critical transition temperature behavior on effective crosslinking density

These observations led us to explore the potential limits of further increasing HA molecular weight. On the one hand, increasing polymer molecular weight is expected to increase entanglements, potentially resulting in a higher density of effective crosslinks and stiffer gels. On the other hand, increasing polymer molecular weight can decrease molecular mobility and cause greater gel defects, leading to less effective crosslinking and weaker gels.[51,85,97] Thus, to further study the role of HA molecular weight, we synthesized sub-families of HELP formulations with 60- and 100-kDa HA. For the 60-kDa sub-family, the gel stiffness increased as the BZA:HYD ratio increased (**Fig. S11**), similar to the trend observed for the 40-kDa HA sub-family of gels. Thus, the 60-kDa HA is also sufficiently long enough to follow the trends predicted by Brachiation theory.

Similar to the 20-kDa HA sub-family, the 100-kDa HA sub-family had a maximum stiffness near a BZA-HYD ratio of 1:1, with decreasing stiffness at lower and higher ratios (**Fig. 3A**). These data suggest that while the 40-kDa and 60-kDa sub-families fit the Brachiation model, as the HA molecular weight is further increased, the presence of network defects and decreased molecular mobility becomes more pronounced, leading to a lower gel stiffness even at high BZA-HYD ratios. The higher susceptibility of 100-kDa formulations to this phenomenon is due to its higher functionality per chain. For example, the 30% modified, 100-kDa HA is estimated to have 75 BZA functional groups per chain, compared to only 45 BZA functional groups for the 30% modified, 60-kDa HA.

This increase in functionality greatly constrains molecular mobility, maintaining the presence of network defects that were formed during initial mixing and rapid crosslinking, which decreases the overall gel stiffness.[72,81-85,95] As with all the HELP sub-families, at higher degrees of modification (20% and 30%), the gelation time was so short that G' was typically larger than G'' by the time rheological data collection was initiated (about 20 seconds after initial mixing) **(Fig. S9)**. We hypothesized that this rapid crosslinking traps the HA polymers into a nonideal network structure, and these defects are maintained for the 100-kDa HA formulations, which have decreased molecular mobility, resulting in lower crosslinking efficiency.[72]

To test this idea, we used temperature to slow down the crosslinking reaction. The ELP-HYD and HA-BZA polymers were mixed and allowed to react for 5 min at 4 °C prior to increasing the temperature to 23 °C for 15 min. As before, all rheological measurements were made at 37 °C. In addition to slowing down the hydrazone crosslinking kinetics, mixing at 4 °C also improves the accessibility of the ELP-HYD functional groups.[21,32,78] As expected, solubilizing the ELP-HYD in 10X iPBS lowers the T_t to slightly below room temperature (~20 °C, **Fig. 3C**). As previously described by others, increasing the phosphate concentration in the buffer solution disrupts the hydration structure surrounding the ELP, leading to a decrease in T_t.[98,99] Thus, by mixing the ELP-HYD below its T_t (~20 °C, Fig. 3C), we allow the protein to be fully hydrated in the solution and adopt an extended, random configuration[98,99] that allows for greater accessibility of reactive sites. Furthermore, the slower reaction kinetics should allow for more homogeneous mixing prior to the onset of gelation and a decrease in network defects. Both of these effects would result in increased crosslinking efficiency and a stiffer gel. Consistent with this hypothesis, mixing the ELP-HYD with the 30% functionalized 100-kDa HA for 5 minutes at 4 °C increased the gel stiffness five-fold compared to mixing at room temperature ($G' \sim$ 1,500 Pa and 300 Pa, respectively, **Fig. 3B**). Interestingly, mixing the sub-family of 100-kDa HA formulations at 4 °C rescued the Brachiation-like

behavior, where gel stiffness increased as BZA-HYD ratio increased. This suggests that the entrapment of the network in a defect-rich state could be overcome by crosslinking the hydrogel at a lower temperature. As many biomaterial hydrogels employ polymers with lower critical solution temperature behavior, including ELP,[32] resilin-like proteins,[100] and poly(N-isopropylacrylamide),[101] this strategy of crosslinking at lower temperatures may be helpful for other systems. Taken together, these data demonstrate that network defects and entanglements can have a pronounced impact on final gel mechanical properties for high molecular weight HA formulations.

There is an upper limit to the contribution of HA entanglements to crosslinking efficiency

To explore the impact of HA entanglements, we compared the gel stiffness for HELP formulations of varying molecular weight and identical degree of BZA functionalization (12%). This 12% degree of modification was selected since it allowed for adequate, homogeneous mixing even for the 100-kDa HA HELP formulation, as evidenced by the similar plateau modulus for gels crosslinked at 23°C and 4°C (Figs. 3A, B). All of these 12% formulations have identical concentrations of crosslinking functional groups, regardless of HA molecular weight (20, 40, 60, 100, 500 kDa) and the same BZA:HYD ratio of 0.8. Thus, the number of potential hydrazone crosslinks formed within the network is theoretically constant. The small increase in stiffness seen from 20 kDa to 40 kDa is expected, as the dynamic polymer network connected pathway becomes longer with an increase in molecular weight (**Fig. 3D**). As we continue to increase the molecular weight to 60 kDa, there is a further increase in stiffness (**Fig. 3D**). This is evidence of longer chains contributing to an increased probability of percolation paths within dynamic hydrogels, as predicted by Brachiation theory (**Fig. 3E**). As the molecular weight is further increased to 100 kDa and 500 kDa, the storage modulus remains relatively constant, suggesting an upper limit to the contribution of entanglements to the crosslinking efficiency.

This observation can be supported by calculating the theoretical entanglement concentration[12,96,102] (c_e) of the HA component in solution by itself. The c_e for 500-kDa HA is around 2.23 wt% (**Table S2**), which is close to the concentration of the HA solution (2 wt%) prior to mixing with the ELP-HYD component. This suggests the solution is already somewhat entangled before mixing and polymer mobility is highly diminished. To check if this diminished mobility might result in insufficient mixing, we compared the plateau storage moduli for gels crosslinked at 23°C and 4°C and found they were similar **(Fig. S12),** suggesting that the 500-kDa, 12% BZA-modified formulation is homogeneous. Thus, although the entanglements can act as physical crosslinks, they also hinder accessibility to available reactive sites and preserve defects within the network. Taken together, these two opposing effects counteract each other; thus, above an upper limit of about 60-Da HA, the gel is not made significantly stiffer by increasing the HA molecular weight. We next sought to understand how entanglements and network defects might impact the injectability and self-healing behavior of these dynamically associating gels.

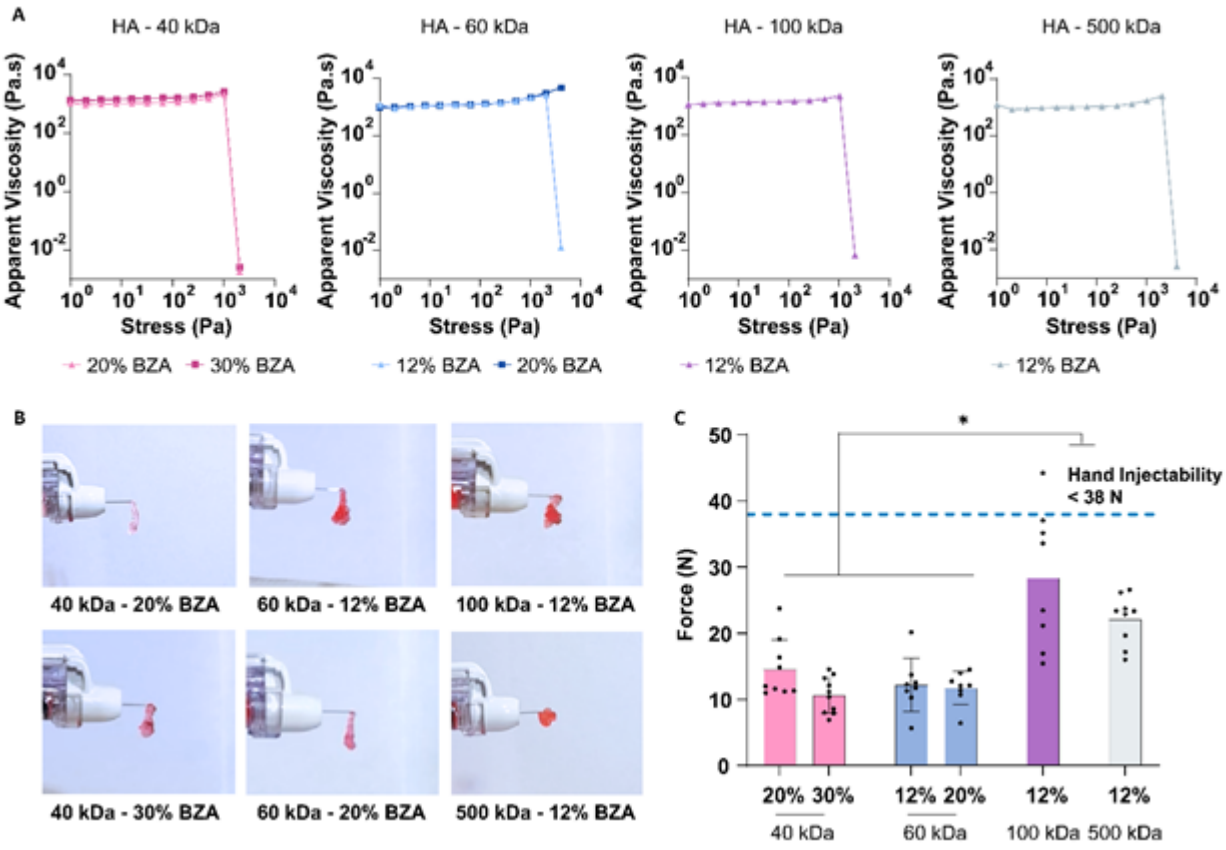

Figure 4. Analysis of gel fracture stress and injectability. A. Fracture stress measurements of HELP formulations with 40, 60, 100, and 500 kDa HA, measured through successive creep tests. Representative of n = 3 plotted. **B.** Photographs of injections of all six gel formulations shown in panel A. **C.** HELP gel extrusion force measured with a load cell and at constant flow rate (0.5 ml/min). N=8-10 for each gel formulation, average +/- standard deviation, one-way ANOVA, all p-values are *p < 0.05, see **Table S3** for specific p-values.

HELP formulations with higher molecular weight HA require higher extrusion forces

In literature, properties such as shear-thinning[103,104] and yield stress[54,105,106] have been shown to govern the extrudability of many physically crosslinked gels. While dynamic crosslinked hydrogels share similar shear-thinning properties, a range of results in injectability has been reported.[65,105,107,108] This variation in injectability has also been observed for different formulations of our HELP system.[10,21,32,109] Similar to other dynamic hydrogels, the HELP hydrogels can undergo fracture during injection, suggesting that plastic deformation and failure are also parameters that must be considered when designing injectable hydrogels.[21,110]

As one of the key advantages of hydrogels is their ability to mimic mechanical features of the native ECM (G' ~1,000 Pa), we focused on systematically assessing the injectability of HELP formulations that are within this stiffness range.[2] Specifically, we investigated the injectability of six HELP formulations spanning four different HA molecular weights: 40-kDa HA, 20 and 30 % BZA, 60-kDa HA, 12 and 20 % BZA, 100-kDa HA, 12 % BZA, and 500-kDa HA, 12 % BZA. First, we evaluated the gel fracture stress and yield stress by performing a series of creep tests with exponentially increasing applied stress, with 1,000 sec recovery time between each test, as previously described.[21,35,111-113] In this testing modality, the fracture stress can be defined as the applied stress that leads to an abrupt decrease in observed viscosity, while the yield stress is defined as the applied stress at which the gel is no longer able to fully return to zero strain within the recovery time.[112] All of the selected formulations were observed to have a fracture stress (σ_f) of similar magnitude (2000 - 5000 Pa), as well as a similar yield stress (σ_y, ~100 Pa) (**Fig. 4A, Fig. S13**).

This range of fracture stress is consistent with previous results, in which HELP formulations with σ_f < 12,000 Pa were extrudable,[21] suggesting all six formulations would be injectable. We empirically assessed the hand-injectability of each selected

formulation, by extruding through a 31-G needle attached to a 1-ml syringe. While all gels were injectable, they appeared to have a fractured morphology immediately after extrusion, suggesting that the gels fracture into discrete microgels before fluidization and are not extruded as a uniform filament (**Fig. 4B**). Similar observations have been reported for other injectable hydrogels, including those formed through peptide assembly.[105,110] HELP formulations with HA of 60 kDa or less were consistently injectable with one hand. However, hydrogels with 100- and 500-kDa HA often required additional effort, with some samples requiring both hands to initiate extrusion through the needle. To systematically quantify this effort, all gels were injected using a syringe pump through a 31-G needle at 0.5 ml/min, and the extrusion force was measured with a load cell (**Fig. S14**). Formulations with HA of 60 kDa or less required about 10 - 15 N, while those with higher molecular weights (100- and 500-kDa) required 20 - 30 N, a two-fold increase in the extrusion force (**Fig. 4C**).

A recent study has correlated hydrogel extrusion force (with a 5-ml syringe fitted to either a 19-G or 31-G needle at 0.2 mm/s and 1 mm/s) with user effort for injection.[114] They showed that study participants considered a gel to be easily injectable if the hand-force required was under 12 N.[114] Gels with extrusion forces from 38 - 64 N were labeled as needing great effort to inject, and extrusion forces above 64 N were not injectable.[114] These published data correlate well with our observations, where formulations with shorter molecular weight HA (60 kDa or less) were relatively easy to inject and had extrusion forces between 10 - 15 N. In contrast, some effort was required to inject formulations with higher molecular weight HA, and measured extrusion forces ranged from 18 – 45 N (**Fig 4C**).

Thus, although these six formulations had similar stiffness, yield stress, and fracture stress, they required different extrusion forces. Interestingly, the hydrogel formulations

that required more effort to inject (e.g. 100- and 500-kDa HA) were also those more susceptible to entanglements and network defects according to our stiffness analysis (**Figs. 2 & 3**). These findings support our hypothesis that chain length and functionality must be considered when formulating injectable hydrogels with DCC. Further, these results suggest that potential clinical applications of HELP hydrogels should use formulations with HA molecular weight of 60 kDa or less, which can provide both stiff mechanics and easy hand-injectability.

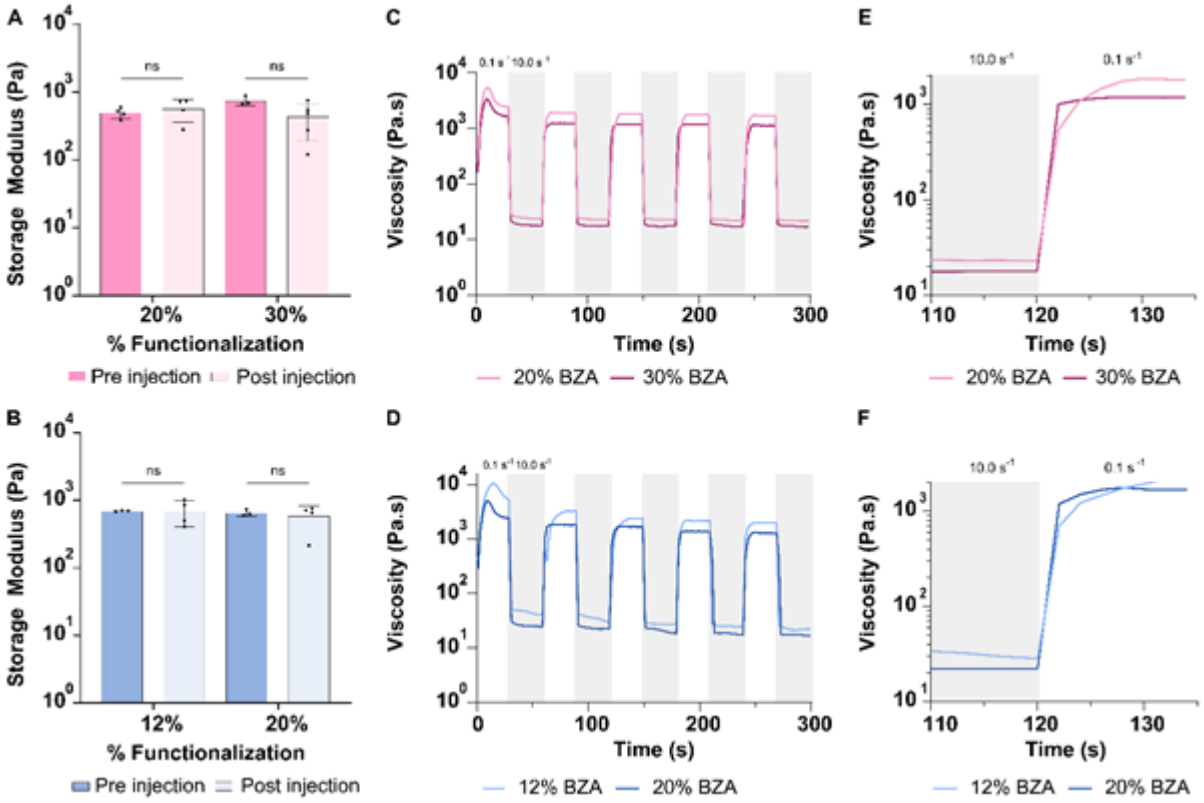

Figure 5. HELP hydrogel mechanics after extrusion. A. Storage modulus of HELP formulations with 40-kDa HA (20 % and 30 % BZA functionalization) before and after syringe-needle injection. **B.** Storage modulus of HELP formulations with 60-kDa HA (12 % and 20 % BZA functionalization) before and after syringe-needle injection. **C.** Viscosity recovery at high (10 s^{-1}) and low (0.1 s^{-1}) shear rates, average of n=3, HELP formulations with 40-kDa HA (20 % and 30 % BZA functionalization). **D.** Viscosity recovery at high (10 s^{-1}) and low (0.1 s^{-1}) shear rates, average of n=3, HELP formulations with 60-kDa HA (12 % and 20 % BZA functionalization). **E.** Viscosity transition from high to low shear rates, HELP formulations with 40-kDa HA (20 % and 30 % BZA functionalization). **F.** Viscosity transition from high to low shear rates, HELP formulations with 60-kDa HA (12 % and 20 % BZA functionalization). One-way ANOVA, n.s. = not significant.

HELP hydrogels quickly self-heal post injection

For many biomedical applications, it is desirable to have an injectable hydrogel rapidly self-heal *in situ*. During self-healing, the material reforms the polymer network and recovers its original mechanical properties.[21,49,54,106,115] In some hydrogels crosslinked with DCC bonds, the transient nature of the DCC bond can allow for the bulk of the hydrogel to shear-thin into a lower viscosity upon application of force, resulting in a gel that is injectable.[116] The DCC bonds then reform after injection to "self-heal," *i.e.,* regain the original mechanical properties. However, the hydrazone bond formed between BZA and HYD moieties highly favors the bonded state (K_{eq} = 1.5 x 10^3), which prevents our gels from extruding in this manner. Instead, the DCC-crosslinked gels reported here are injectable through a process of microgel fracture,[21] which has also been reported for other hydrogels including peptide- and protein-based materials.[105,110] This behavior is why the HELP gels visibly break into discrete gel fragments upon extrusion (**Fig. 4B**). Previously, injectability that occurs through microgel fracture has been associated with rapid self-healing behavior. This is because the polymer network within the microgel

fragments is relatively undisturbed, and only a few bonds must re-form between the interfaces of the microgel fragments to self-heal into a continuous network. In contrast, for hydrogels that undergo bulk shear-thinning, the entire polymer network must re-form,[104] a process that can take significant time. Thus, we hypothesize that after injection, the HELP hydrogels should be able to quickly regain their stiffness and demonstrate similar mechanical behavior pre- and post-injection.

To test this hypothesis, we analyzed the mechanical properties post-extrusion of HELP formulations that are stiff (~1,000 Pa), yet easily hand-injectable (i.e., formulations with 40-kDa and 60-kDA HA). Each of these formulations (40-kDa HA, 20 % and 30 % BZA; 60-kDa HA, 12 % and 20 % BZA) was prepared within a 1-ml syringe with a 31-G needle and allowed to gel for 1 hour at room temperature. Then, the hydrogels were extruded directly onto the rheometer stage for mechanical characterization.

We allowed the gel to recover for up to 1 hour at 1 % strain and 37 °C to simulate body temperature, during which time we observed a slight increase in the storage modulus, with the storage modulus consistently higher than the loss modulus (**Fig. S15**). This indicated that the network reformed, healing the fractured structure into a cohesive hydrogel network. Next, we performed a frequency sweep (0.1 to 100 rad/s) at high strain (10 %) to evaluate the final storage modulus and validate that the hydrogel was still in the linear viscoelastic regime. All formulations were able to withstand these high strains and did not show statistically significant differences in stiffness when compared to the pre-injection hydrogels at the same conditions (**Fig. 5A and B**).

Interestingly, the degree of functionalization, within each subfamily, appeared to have an impact on the kinetics of self-healing, which can be observed in the viscosity

response when alternating between high (10 s^{-1}) and low (0.1s^{-1}) shear rates (**Fig. 5C-F**). All tested HELP hydrogels displayed reproducible viscous shear-thinning and self-healing behavior, as expected (**Fig. 5C and D**). In addition, looking closer at the viscosity response at the transition between high and low shear rates (**Fig. 5E and F**), we can distinctly observe the faster plateau of viscosity for formulations with a higher degree of functionality (*i.e.,* 40-kDa HA at 30 % BZA; 60-kDa HA at 20 % BZA). Taken together, this supports our hypothesis that the dynamic crosslinks allow the gel to rapidly recover its mechanical properties.

HELP hydrogels have clinical potential as minimally-invasive delivery systems

Injection is a favorable route for delivery of therapies, including cells and pharmaceuticals, for many different medical indications.[5,117,118] While many tissues can be directly accessed by a syringe needle, other indications such as myocardial infarction and neurovascular blockages require local delivery through the use of catheters. The potential extrudability of hydrogels will depend on the geometry of the device (i.e. diameter, length) through which it is extruded.[103,119] Specifically, the applied pressure required to extrude a material (including physical hydrogels) will be directly proportional to the length of the channel and inversely proportional to the radius of the channel[103,119] Since catheters can be substantially longer (~1.5 m) and narrower (~10^{-2} m) than a syringe, not all hydrogels that are hand-injectable through a syringe are injectable through a catheter.[120]

Therefore, to evaluate the potential for clinical delivery through a minimally-invasive catheter, we injected two HELP formulations through a long, thin cannula with length of 2 m and an inner diameter of 250 μm, longer and thinner than several clinically employed catheters. The HELP formulation with 40-kDa HA and 20 % BZA functionalization (**Fig. S16**) and the formulation with 60-kDa HA and 20 % BZA (**Fig.**

1E) were both injectable using only hand force and were observed to re-form into a gel after extrusion through the cannula.

3. Conclusion

Dynamic covalent crosslinked hydrogels have great potential for use as cell culture platforms, tissue engineering scaffolds, and therapeutic delivery. Further, their tunable mechanics and capacity for injectability allow for simple translation into many medical applications. Nonetheless, more exploration is necessary to uncover the fundamental design rules that allow formulation of DCC hydrogels that are injectable and have robust mechanics.

To investigate the molecular parameters that might impact injectability, we developed a family of ELP and HA dynamic gels crosslinked through hydrazone bonds. Specifically, we varied the molecular weight of the HA and its degree of functionalization with the BZA moiety. In general, gelation time rapidly decreased with an increase in degree of functionalization within each molecular-weight subfamily. This rapid crosslinking leads to nonideal network formation and increases the presence of defects. However, concurrent with this effect, we also observed that increasing HA molecular weight increased the hydrogel stiffness, due to chain entanglements and longer percolation paths through the network, creating a more effectively crosslinked gel. Overall, these two effects appear to offset each other. For lower HA molecular weights, the percolation paths and entanglements are limited, so defect formation dominates at higher HA functionalities. This phenomenon is observed in our 20-kDa HA subfamily, which presents its lowest stiffness at its highest degree of functionalization (**Fig. 2B**). However, in formulations with higher HA molecular weights, entanglements and longer percolation paths have a larger contribution to the network, leading to an increase in

stiffness. This is observed in our 40-kDa and 60-kDa HA subfamilies, where the highest stiffness corresponds to the highest degree of functionalization (**Fig. 2D, S11**).

In a complementary analysis, we held the degree of functionalization constant and evaluate the impact of changing HA molecular weight. In general, longer HA chains lead to greater entanglements and longer percolation paths, resulting in stiffer hydrogels (**Fig. 3D**). However, we also observed an upper limit to this effect, as further increasing HA molecular weight to 100 kDa and higher did not further increase gel stiffness. This is likely due to the diminished molecular mobility in highly entangled solutions, which compromises the uniformity of the network. Interestingly, this behavior is predicted by Brachiation theory, a recent model developed by Cai *et al*. to describe dynamically associating polymer networks. In the Brachiation model, longer chains increase the likelihood of chain entanglements and chain-spanning across the network, which is in agreement with our observed experimental data. Further, Brachiation theory also predicts that chains with higher functionalization have decreased mobility, consistent with our observations of decreased gelation time.

Having evaluated the effects of HA functionality and molecular weight on the mechanics of our family of hydrogels, we then aimed to elucidate their impact on gel injectability. All of the tested gels were visibly fractured immediately after injection, suggesting that injectability occurs through microgel fracture. While rheological studies quantified similar fracture and yield stresses across all tested formulations, their extrusion forces had significant differences. Lower molecular weight HA formulations (60-kDa and below) had extrusion forces nearly half that of higher molecular weight HA formulations (**Fig. 4C**). This is consistent with our hypothesis that the uniformity of the polymer network has a direct impact on gel injectability, as this higher force is likely a direct effect of the entanglements that are more prevalent in the higher molecular

weight HA formulations. To demonstrate potential clinical translatability of our stiffer formulations (G'~1,000 Pa), they were extruded by hand-force through a long, thin cannula to simulate catheter delivery. Finally, we showed that the dynamic crosslinks in the HELP hydrogel (formulations with 40-kDa and 60-kDa HA) reformed the polymer network post injection, allowing the gels to self-heal and regain the original mechanical properties. For this analysis, we found that increasing the HA functionalization resulted in more rapid self-healing. While this is true for our formulations with intermediate molecular weight HA, exploring the recovery kinetics for larger molecular weight polymers whose entanglements may hinder self-healing is an interesting topic for future investigation.

Taken together, we have demonstrated the need to consider both the degree of functionalization and polymer molecular weight to achieve stiff, yet hand-injectable and self-healing DCC hydrogels. Our results suggest that future efforts to design injectable DCC gels should focus on formulations with a degree of functionalization similar to the crosslinking reaction stoichiometry (for our system, a 1:1 ratio of BZA:HYD). This allows optimal chemical crosslinking to occur and limits defect formation during the rapid gelation of high functionality systems. Additionally, our results encourage the use of medium-sized molecular weight polymers when formulating injectable DCC hydrogels. Intermediate polymer chain lengths are long enough to form percolating paths through the network without compromising molecular mobility; furthermore, longer chain lengths can cause entanglements that significantly inhibit injectability. In summary, by exploring the structure-function relationships between polymer molecular weight, polymer functionalization, and gel material properties, we have increased understanding of how to formulate injectable DCC hydrogels, greatly increasing their clinical potential for future medical applications.

4. Materials and Methods

Materials: Unless otherwise noted, all reagents were purchased from Sigma-Aldrich and used without further purification.

Synthesis of elastin-like protein (ELP). The elastin-like protein (ELP) was synthesized through recombinant protein expression as previously described.[39] Briefly, plasmids encoding the ELP amino acid sequence (**Fig. S1**) were transformed into BL21(DE3) pLysS *Escherichia coli* (Life Technologies). The bacteria were grown in Terrific Broth at 37 °C, up to an OD_{600} of 0.8, at which point ELP expression was induced by adding 1 mL of 1 M isopropyl β-D-1-thiogalactopyranoside (IPTG, Fisher), for a final concentration of 1 x 10^{-3} M. Expression continued for 7 h, after which the bacteria were pelleted and resuspended in TEN Buffer (10 × 10^{-3} M Tris (Fisher), 1 × 10^{-3} M EDTA (Fisher), and 100 × 10^{-3} M NaCl (Fisher), pH 8.0). The pellet was lysed through three alternating freeze (-80 °C) and thaw (4 °C) cycles. Deoxyribonuclease (DNAse) and phenylmethylsulphonyl fluoride (PMSF) were added to the cell lysate at 1 × 10^{-3} M, to degrade DNA and inhibit proteolysis, respectively. ELP was purified through cold (4 °C) and hot (37 °C) spin thermocycling, dialyzed in deionized water (DI) for three days at 4 °C, changing water 2 to 3 times a day and using 3.5 kDa MWCO dialysis tubing (Spectrum Labs 132576). The solution was then frozen, lyophilized, and stored at -20 °C.

Functionalization and Characterization of ELP with Hydrazine (ELP-HYD): The ELP was modified following previously published protocols,[21,32,34] by modifying the amine on the lysine amino acid. In summary, the lyophilized ELP was dissolved in a 1:1 solution of anhydrous dimethyl sulfoxide (DMSO) and N,N-dimethylformamide (DMF) at a 3% (w/v). Tri-Boc hydrazinoacetic acid (Tri-boc, 2 equivalence per ELP amine) was dissolved in anhydrous DMF at 2.1 % (w/v), in a separate reaction vessel at room temperature. Once dissolved, the tri-boc was activated with hexafluorophosphate

azabenzotriazole tetramethyl uronium (HATU; 2.0 equivalence per ELP amine; Sigma, 445460) and 4-methylmorpholine (NMM, 5 equivalence per ELP amine). After 10 minutes, the activated tri-boc was added to the ELP in a drop-wise manner while continuously stirring. The reaction was left to proceed overnight, under constant stirring at room temperature. The modified protein was then precipitated by adding the solution dropwise in ice-cold diethyl ether in a 1:4 volume ratio of ELP solution to ether. The product was pelleted and dried under nitrogen overnight. To deprotect the hydrazine functional group, the ELP pellets were resuspended in a 1:1 solution of dichloromethane (DCM) and trifluoroacetic acid (TFA) with 5% (v/v) tri-isopropylsilane (Sigma, 233781) for 4 hours under continuous stirring at room temperature. The deprotected ELP-HYD was precipitated in ether, dried under nitrogen overnight, and resuspended in DI water prior to dialyzing for three days at 4 °C, changing water 2 to 3 times a day and using 3.5 kDa MWCO dialysis tubing (Spectrum Labs 132576). The resulting solution was then filtered (0.22 μm) and lyophilized, resulting in a fibrous white solid, which was stored at -20 °C.

Synthesis of azidopropyl-benzaldehyde (Azido-BZA): To prepare the small molecule for the click-chemistry reaction, we modified 4-formylbenzoic acid (Sigma-Aldrich 124915-25G) in two steps, as previously described.[33] Briefly, 4-formylbenzoic acid was dissolved in extra dry dichloromethane (DCM, Acros Organics 61030-0010), and N-hydroxysuccinimide (NHS, 1.1 equivalence to 4-formylbenzoic acid) and 1-(3-dimethylaminopropyl)-3-ethylcarbodiimide hydrochloride (EDC, 1.1 equivalence to 4-formylbenzoic acid) were added to the reaction vessel. The reaction was allowed to proceed at room temperature overnight while stirring. The reaction was diluted in an equal volume of DCM (Fisher Chemical D151-4) and transferred to a separatory funnel, in which an equal volume of water was added to remove water-soluble byproducts. The organic phase was collected, and this washing step was performed two additional times with DI water, followed by two washes with brine solution (178.5 g sodium chloride / L

DI water). The organic phase was collected, and magnesium sulfate ($MgSO_4$, Sigma-Aldrich 793612-500G) was added to absorb any remaining water. The solution was filtered and concentrated through a rotary evaporator, resulting in a white fluffy powder of NHS-benzaldehyde. The NHS-benzaldehyde (NHS-BZA) was redissolved in dry DCM. 3-azidopropylamine (Click Chemistry Tools AZ115-1000, 1.5 equivalence to NHS-BZA) and diisopropyl ethyl amine (DIPEA; Sigma Aldrich D125806-100ML, 3 equivalence to NHS-BZA), a catalytic base, were added. The reaction proceeded for 24 hours at room temperature, capped, and stirring. The same washing steps of water and brine and $MgSO_4$ were performed. The product was purified through a silica (Sigma-Aldrich 60737-1KG) column in a mobile phase of 10:1 DCM:Acetone (Thermo Fisher A18-4). Conversion into the final product, azido-propylbenzaldehyde (azido-BZA), was verified through thin-layer chromatography (TLC silica gel, Millipore Sigma 105534.0001).

Functionalization and Characterization of Hyaluronic Acid with Benzaldehyde (HA-BZA): Hyaluronic acid (HA) was functionalized following previously published protocols.[21,33] First, HA was modified with an alkyne group. Hyaluronic acid sodium salt (LifeCore, HA20K-1, HA40K-1, HA60K-1, HA100K-1, HA500K-1) was dissolved in MES buffer (0.2 M MES hydrate (Sigma Aldrich M2933-100G), 0.15 M NaCl in water; pH 4.5) to a 1 wt% solution. Propargylamine (Sigma Aldrich P50900-5G) was added to the reaction vessel at equivalences (eq.) depending upon the final BZA functionalization and the pH was adjusted to 6 (1 eq. for 6 and 12 % BZA functionalization, 3 eq. for 20% BZA functionalization, and 6 eq. for 30 % BZA functionalization). NHS and EDC were added at the equimolar amount to BZA functionalization, and the reaction was stirred at room temperature overnight. The final mixture was dialyzed for three days against DI water, changing water 2 to 3 times a day, using 3.5 kDa MWCO dialysis tubing (Spectrum Labs 132576). After dialysis, the mixture was filtered through a 0.22 μm filter and lyophilized, resulting in a white fibrous material of HA-alkyne (**Fig. S3**).

As the final step to obtaining HA-BZA, the HA-alkyne solid was dissolved in isotonic 10x PBS (10X iPBS) (81 mM sodium phosphate dibasic, 19 mM sodium phosphate monobasic, 60 mM sodium chloride in Milli-Q water; pH adjusted to 7.4; 0.22 μm filtered) supplemented with beta-cyclodextrin (Sigma C4767-25G) at a 1 mg/mL. Stock solutions of 2.4 mM copper sulfate (Copper sulfate, 5-hydrate - JT Baker 1841-01) and 45.2 mM sodium ascorbate (Sodium L-ascorbate - Sigma A7631-100G) were prepared. All solutions were degassed for 30 minutes under nitrogen. Finally, azido–BZA was dissolved in extra dry dimethyl sulfoxide (DMSO, Acros Organics 61097-1000) depending on the targeted BZA functionalization: 1 eq. with respect to the corresponding HA-alkyne for 6 % BZA functionalization, and 2 eq. for 12, 20, and 30 % BZA functionalization. Then, the sodium ascorbate and copper sulfate solutions were added sequentially through an insulin syringe to the reaction vessel for a final concentration of 452 μM and 24 μM, respectively. Finally, azido-BZA was added and the final solution was degassed for 10 minutes. The reaction was left stirring for 24 hours at room temperature. After 24 hours, an equal volume of 50 mM Ethylenediamine Tetraacetic Acid Disodium Salt Dihydrate (EDTA, Fisher O2793-500) at pH 7.0, was added to chelate the copper from the reaction and allowed to stir for 1 hour. Finally, the mixture was dialyzed, filtered, and lyophilized as previously described, resulting in a white fibrous solid. The final HA-BZA was characterized through H^1 NMR,[21,33] and the different degrees of functionalization were quantified, resulting in (6 ± 3%, 12 ± 3%, 20 ± 3%, 30 ± 3%) (**Fig. S4 - S8**).

Hydrogel formation: All HELP hydrogels have a final composition of 1 wt % ELP-HYD and 1 wt% HA-BZA in 10x iPBS (10X Isotonic PBS: 81 mM sodium phosphate dibasic, 19 mM sodium phosphate monobasic, 60 mM sodium chloride in Milli-Q water; pH adjusted to 7.4; 0.22 μm filtered), regardless of the HA molecular weight or degree of functionalization. The components, HA-BZA and ELP-HYD, were dissolved at stock

concentration of 2 wt% in isotonic 10x PBS overnight at 4 °C under continuous rotation. Equal volumes of 2 wt% HA-BZA and 2 wt% ELP-HYD were mixed on ice, to prevent ELP aggregation. This procedure allowed for the hydrazone crosslinks to spontaneously form, creating the final gels with final concentration of 1 wt% HA and 1 wt% ELP.

Rheological Measurements: Stress-controlled ARG2 rheometer (TA Instruments) using a 20-mm diameter, cone-on-plate geometry, was used to perform all rheological analysis. To prevent evaporation, a layer of heavy mineral oil was placed between the stage and the cone-on-plate geometry for all measurements.

Gelation time and storage modulus: We performed a time-sweep at 1 % strain and 1.0 rad/s for 15 minutes at 23 °C, to allow for gelation at room temperature with the least disturbance possible. Gelation time at 1.0 rad/s was defined as the point in which the storage modulus (G') becomes larger than the loss modulus (G'') (tan $\delta \leq 1$) for 40 consecutive seconds to account for noise on the recording.[74-77] This was followed by a temperature ramp to 37 °C at a rate of 3 °C per min, in which the gel was allowed to equilibrate in a time sweep for 15 to 30 minutes, in which we saw the plateau in storage modulus, (**Fig. S10**). The storage modulus of the gel was assessed in a frequency sweep at 1 % strain from 0.1 to 100 rad/s, and the modulus reported at 1.0 rad/s. For pre- and post-injection comparisons, the storage modulus was assessed at 10% strain, and reported at 1.0 rad/s.

To assess the impact of rapid crosslinking on 100 kDa-HA HELP formulations, we added a 5-minute time-sweep at 4 °C, also at 1.0 rad/s and 1% strain, followed by a temperature ramp to 23 °C, to the beginning of the protocol described above. Stiffness was reported at 1.0 rad/s and 1 % strain at 37 °C.

Yield and Fracture stress: As before, the hydrogels were allowed to gel for 30 minutes at 23 °C, and gelation was confirmed by a frequency sweep at 1% strain, from 0.1 to 10 rad/s. Then, we evaluated the gel yield and fracture stress by performing a series of creep tests with exponentially increasing applied stress with 1,000 seconds of recovery time between each test, as previously described.[21,35,111-113] Here, the recovery time accounts for the relaxation present due to the hydrogel's viscoelasticity. In the elastic regime, before yielding, complete strain recovery is observed upon the removal of the applied stress.[111,112] Yield stress was defined as the applied stress in which the strain does not fully recover after removing the applied stress, even after the end of recovery time, indicated by the presence of non-zero plastic strain, e.g., yielding (permanent deformation).[111,112] Fracture stress was defined as the applied stress in which the measured strain increased rapidly and indefinitely, indicating the hydrogel had fractured (measured strain > 2000%, e.g., all gels failed at strains < 2000%) and the geometry was rotating freely, at which point, the creep test was terminated.

To validate this procedure as an effective method for measuring fracture stress, we applied newton's law of viscosity, below, where σ is the applied stress, η_{apparent} is the apparent viscosity, γ and $\dot{\gamma}$ are the shear strain and shear rate respectively. By plotting the apparent viscosity with respect to the applied stress (**Fig. 5A**), we observe an abrupt decrease in viscosity is observed, as the strain sharply increases.

$$\sigma = \eta_{\text{apparent}} \times \dot{\gamma} \qquad \& \qquad \dot{\gamma} = \frac{\gamma}{t}$$

Our initial creep test had an applied stress of 1 Pa for 3 minutes, followed by 1,000 seconds of recovery at zero-stress to allow for the viscoelastic material to relax. The next creep test was at 2 Pa, followed by the same recovery time. We continued this repetition increasing the applied stress exponentially, i.e. 1, 2, 4, 8, 16 Pa…, up to the

point where the measured strain increased towards "infinity", indicating the gel had fractured.

Some creep tests at higher applied stresses were immediately terminated, collecting a single data point. This indicates that, in these instances, the strain went quickly over the fracture threshold (measured strain > 2000%) and the test was terminated, suggesting brittle failure.[21] The fracture stress, (**Fig. S13**), is an average of n = 3 – 5 of the applied stress value at which the test was terminated. We observed a nearly constant apparent viscosity for all formulations, indicating a Newtonian behavior, followed by a sudden dip towards "zero viscosity" – indicating the strain increased towards "infinity". Therefore, we can conclude the gel fractured at the specific applied stress.[21]

Hydrogel preparation for injectability assessment: To assess the injectability of our material, we injected the gels through 1ml, 31 G insulin syringes (Becton Dickinson). The two polymer stock solutions and the syringes were kept in ice for 10 minutes before hydrogel formation, to ensure complete solubility of ELP. Then, holding the syringe horizontally, we loaded 25 μL of each component, 2 wt% HA-BZA and 2 wt% ELP-HYD, through the back of the syringe.[21] Then, we carefully placed the plunger and tilted the syringe upright, moving the plunger up-down 15 to 20 times to fully mix the hydrogel. During mixing, care was taken to avoid pushing the hydrogel into the needle, which could clog it. The syringe was placed on ice for 30 seconds after mixing, to prevent the ELP from crashing out due to the heat from the friction. Then, the loaded syringe was allowed to gel at room temperature for 45 to 60 minutes, ensuring full gelation of the final 50 μL HELP hydrogel.

Extrusion force measurements: The extrusion force was measured through a load cell (LCKD-500; Omegadyne, Sunbury, OH, F = 0 – 2224 N) coupled to a syringe pump (SyringeONE:100, New Era Instruments)[118] through a 3D printed adaptor, (**Fig. S14**). As directed by the manufacturer, the load cell was calibrated with a calibrating weight of 1 kg (9.81 N), and the output was displayed in newtons (N). The hydrogels were prepared within the syringes as previously discussed; however, the component volumes were increased to 50 µL each. For better visualization of the extruded gel, 0.5 µL of red food coloring was added to the hydrogel. The 100 µL hydrogels were mixed and allowed to gel at room temperature for 45 – 60 min, and then mounted on the syringe pump and injected at 0.5 mL/min. The maximum force displayed for each sample was recorded as the extrusion force.[118] Each formulation had 8 to 10 replicates.

Post-injection mechanical properties: To assess the mechanical properties of our hydrogels post-injection, we formed the hydrogel inside the 1 ml 31 G syringe as described above and injected directly on the rheometer's stage at 37 °C to match body temperature. We allowed the gel to equilibrate and recover post-injection for 15 - 60 minutes, in a time-sweep at 1 rad/s and 1% strain, (**Fig. S15**). To evaluate the stiffness and resistance to high strain, the gels were subjected to a frequency sweep at 10 % strain from 0.1 to 100 rad/s, and the modulus reported at 1 rad/s. Next, we analyzed the shear-thinning and self-healing by performing flow peaks, holding for 30 seconds at alternating shear rates 0.1 1/s (low) and 10.0 1/s (high), similar to previously published protocols[106,121-124]. Here, shear-thinning and self-healing data is shown as an average of n=3.

Statistical Analysis: For all figures, data is presented as the mean and standard deviation. Individual replicates are represented as black points, where appropriate. Prior to significance testing, normality and equality of variance were tested with Shapiro–Wilks,

Normal QQ plots, and Brown–Forsythe at significance level 0.05, respectively. All data was analyzed through an unbalanced one-way ANOVA, and Tukey's post-hoc means comparison at significance level 0.05. Outlier tests were conducted with ROUT, at Q = 1%. No outliers were identified. All significance is denoted as *p < 0.05, **p< 0.01, ***p < 0.001, ****p < 0.0001 and ns as not significant. All analysis was performed with GraphPad Prism9.

Disclosures/Conflict of Interest

None

Author Contributions

Narelli de Paiva Narciso: conceptualization, methodology, investigation, formal analysis, data curation, visualization, writing – original draft. Renato S. Navarro: conceptualization investigation, writing – review & editing, resources. Aidan Gilchrist: conceptualization, formal analysis, writing – review & editing, resources. Miriam L. M. Trigo: methodology, investigation. Giselle Aviles Rodriguez: investigation. Sarah C. Heilshorn: conceptualization, writing – review & editing, supervision, funding acquisition.

Acknowledgements

We acknowledge R. Suhar, N. Baugh, and P. Cai for rheological measurements training and assistance and helpful conversations. This work was supported by the National Institutes of Health (NIH) R01 EB027666, **R01 EB027171, R01 HL142718**, and R01 HL151997 and the National Science Foundation (NSF) **CBET 2033302** to S.C.H, by the American Heart Association Postdoctoral Fellowship (903771) to R.S.N, and Foothill College Science Learning Institute for GAR.

References

1. Cascone S, Lamberti G. Hydrogel-based commercial products for biomedical applications: A review. *Int J Pharm*. Jan 5 2020;573:118803. doi:10.1016/j.ijpharm.2019.118803

2. Chaudhuri O, Cooper-White J, Janmey PA, Mooney DJ, Shenoy VB. Effects of extracellular matrix viscoelasticity on cellular behaviour. *Nature*. Aug 2020;584(7822):535-546. doi:10.1038/s41586-020-2612-2

3. Bretherton RC, Deforest CA. The Art of Engineering Biomimetic Cellular Microenvironments. *ACS Biomaterials Science & Engineering*. 2021;7(9):3997-4008. doi:10.1021/acsbiomaterials.0c01549

4. Tang SC, Richardson BM, Anseth KS. Dynamic covalent hydrogels as biomaterials to mimic the viscoelasticity of soft tissues. *Prog Mater Sci*. Jul 2021;120doi:ARTN 100738

10.1016/j.pmatsci.2020.100738

5. Zhou H, Liang CY, Wei Z, et al. Injectable biomaterials for translational medicine. *Materials Today*. Sep 2019;28:81-97. doi:10.1016/j.mattod.2019.04.020

6. Lou H, Feng M, Hageman MJ. Advanced Formulations/Drug Delivery Systems for Subcutaneous Delivery of Protein-Based Biotherapeutics. *J Pharm Sci*. Nov 2022;111(11):2968-2982. doi:10.1016/j.xphs.2022.08.036

7. Franco-Valencia K, Nóbrega IBC, Cantaruti T, et al. Subcutaneous injection of an immunologically tolerated protein up to 5 days before skin injuries improves wound healing. *Brazilian Journal of Medical and Biological Research*. 2022;55doi:10.1590/1414-431x2021e11735

8. Zhang Y, Yu J, Kahkoska AR, Wang J, Buse JB, Gu Z. Advances in transdermal insulin delivery. *Adv Drug Deliv Rev*. Jan 15 2019;139:51-70. doi:10.1016/j.addr.2018.12.006

9. Guimaraes TACD, Georgiou M, Bainbridge JWB, Michaelides M. Gene therapy for neovascular age-related macular degeneration: rationale, clinical trials and future directions. *British Journal of Ophthalmology*. 2021;105(2):151-157. doi:10.1136/bjophthalmol-2020-316195

10. Yang H, Qin X, Wang H, et al. An in Vivo miRNA Delivery System for Restoring Infarcted Myocardium. *ACS nano*. Sep 24 2019;13(9):9880-9894. doi:10.1021/acsnano.9b03343

11. Rybakova Y, Kowalski PS, Huang Y, et al. mRNA Delivery for Therapeutic Anti-HER2 Antibody Expression In Vivo. *Molecular Therapy*. 2019;27(8):1415-1423. doi:10.1016/j.ymthe.2019.05.012

12. Rubinstein M, Colby RH, Knovel. *Polymer physics*. Oxford University Press; 2003:1 online resource (xi, 440 p.).

13. Muir VG, Burdick JA. Chemically Modified Biopolymers for the Formation of Biomedical Hydrogels. *Chem Rev*. Sep 22 2021;121(18):10908-10949. doi:10.1021/acs.chemrev.0c00923

14. Dimatteo R, Darling NJ, Segura T. In situ forming injectable hydrogels for drug delivery and wound repair. *Adv Drug Deliv Rev*. Mar 1 2018;127:167-184. doi:10.1016/j.addr.2018.03.007

15. Domingues RM, Silva M, Gershovich P, et al. Development of Injectable Hyaluronic Acid/Cellulose Nanocrystals Bionanocomposite Hydrogels for Tissue Engineering Applications. *Bioconjug Chem*. Aug 19 2015;26(8):1571-81. doi:10.1021/acs.bioconjchem.5b00209

16. Richardson BM, Wilcox DG, Randolph MA, Anseth KS. Hydrazone covalent adaptable networks modulate extracellular matrix deposition for cartilage tissue engineering. *Acta Biomater*. Jan 1 2019;83:71-82. doi:10.1016/j.actbio.2018.11.014

17. Rosales AM, Anseth KS. The design of reversible hydrogels to capture extracellular matrix dynamics. *Nat Rev Mater*. 2016;1doi:10.1038/natrevmats.2015.12

18. Baker AEG, Bahlmann LC, Tam RY, et al. Benchmarking to the Gold Standard: Hyaluronan-Oxime Hydrogels Recapitulate Xenograft Models with In Vitro Breast Cancer Spheroid Culture. *Adv Mater*. Sep 2019;31(36):e1901166. doi:10.1002/adma.201901166

19. Burdick JA, Prestwich GD. Hyaluronic acid hydrogels for biomedical applications. *Adv Mater*. Mar 25 2011;23(12):H41-56. doi:10.1002/adma.201003963

20. Han Y, Cao Y, Lei H. Dynamic Covalent Hydrogels: Strong yet Dynamic. *Gels*. Sep 10 2022;8(9)doi:10.3390/gels8090577

21. Suhar RA, Doulames VM, Liu Y, et al. Hyaluronan and elastin-like protein (HELP) gels significantly improve microsphere retention in the myocardium. *Biomater Sci*. May 17 2022;10(10):2590-2608. doi:10.1039/d1bm01890f

22. De France KJ, Cranston ED, Hoare T. Mechanically Reinforced Injectable Hydrogels. *ACS Applied Polymer Materials*. 2020/03/13 2020;2(3):1016-1030. doi:10.1021/acsapm.9b00981

23. Rumon MMH, Sarkar SD, Uddin MM, et al. Graphene oxide based crosslinker for simultaneous enhancement of mechanical toughness and self-healing capability of conventional hydrogels. *RSC Adv*. Mar 1 2022;12(12):7453-7463. doi:10.1039/d2ra00122e

24. Taylor DL, In Het Panhuis M. Self-Healing Hydrogels. *Adv Mater*. Nov 2016;28(41):9060-9093. doi:10.1002/adma.201601613

25. Wang W, Narain R, Zeng H. Rational Design of Self-Healing Tough Hydrogels: A Mini Review. *Front Chem*. 2018;6:497. doi:10.3389/fchem.2018.00497

26. Urosev I, Bakaic E, Alsop RJ, Rheinstadter MC, Hoare T. Tuning the properties of injectable poly(oligoethylene glycol methacrylate) hydrogels by controlling precursor polymer molecular weight. *J Mater Chem B*. Oct 28 2016;4(40):6541-6551. doi:10.1039/c6tb02197b

27. Steinman NY, Bentolila NY, Domb AJ. Effect of Molecular Weight on Gelling and Viscoelastic Properties of Poly(caprolactone)-b-Poly(ethylene glycol)-b-Poly(caprolactone) (PCL-PEG-PCL) Hydrogels. *Polymers (Basel)*. Oct 15 2020;12(10)doi:10.3390/polym12102372

28. Zawaneh PN, Singh SP, Padera RF, Henderson PW, Spector JA, Putnam D. Design of an injectable synthetic and biodegradable surgical biomaterial. *Proc Natl Acad Sci U S A*. Jun 15 2010;107(24):11014-9. doi:10.1073/pnas.0811529107

29. Kopac T, Rucigaj A, Krajnc M. The mutual effect of the crosslinker and biopolymer concentration on the desired hydrogel properties. *Int J Biol Macromol*. Sep 15 2020;159:557-569. doi:10.1016/j.ijbiomac.2020.05.088

30. Rodell CB, Dusaj NN, Highley CB, Burdick JA. Injectable and Cytocompatible Tough Double-Network Hydrogels through Tandem Supramolecular and Covalent Crosslinking. *Adv Mater*. Oct 2016;28(38):8419-8424. doi:10.1002/adma.201602268

31. GhavamiNejad A, Ashammakhi N, Wu XY, Khademhosseini A. Crosslinking Strategies for 3D Bioprinting of Polymeric Hydrogels. *Small*. Sep 2020;16(35):e2002931. doi:10.1002/smll.202002931

32. Wang H, Zhu D, Paul A, et al. Covalently adaptable elastin-like protein - hyaluronic acid (ELP - HA) hybrid hydrogels with secondary thermoresponsive crosslinking for injectable stem cell delivery. *Adv Funct Mater*. Jul 26 2017;27(28)doi:10.1002/adfm.201605609

33. Lesavage BL, Gilchrist AE, Krajina BA, et al. Engineered extracellular matrices reveal stiffness-mediated chemoresistance in patient-derived pancreatic cancer organoids. Cold Spring Harbor Laboratory; 2022.

34. Hunt DR, Klett KC, Mascharak S, et al. Engineered Matrices Enable the Culture of Human Patient-Derived Intestinal Organoids. *Adv Sci (Weinh)*. May 2021;8(10):2004705. doi:10.1002/advs.202004705

35. Hull SM, Lou J, Lindsay CD, et al. 3D bioprinting of dynamic hydrogel bioinks enabled by small molecule modulators. *Sci Adv*. Mar 31 2023;9(13):eade7880. doi:10.1126/sciadv.ade7880

36. Tous E, Ifkovits JL, Koomalsingh KJ, et al. Influence of injectable hyaluronic acid hydrogel degradation behavior on infarction-induced ventricular remodeling. *Biomacromolecules*. Nov 14 2011;12(11):4127-35. doi:10.1021/bm201198x

37. Xu X, Jha AK, Harrington DA, Farach-Carson MC, Jia X. Hyaluronic Acid-Based Hydrogels: from a Natural Polysaccharide to Complex Networks. *Soft Matter*. 2012;8(12):3280-3294. doi:10.1039/C2SM06463D

38. Rodell CB, Wade RJ, Purcell BP, Dusaj NN, Burdick JA. Selective Proteolytic Degradation of Guest-Host Assembled, Injectable Hyaluronic Acid Hydrogels. *ACS Biomater Sci Eng*. Apr 13 2015;1(4):277-286. doi:10.1021/ab5001673

39. LeSavage BL, Suhar NA, Madl CM, Heilshorn SC. Production of Elastin-like Protein Hydrogels for Encapsulation and Immunostaining of Cells in 3D. *J Vis Exp*. May 19 2018;(135)doi:10.3791/57739

40. Yang H, Qin X, Wang H, et al. An in Vivo miRNA Delivery System for Restoring Infarcted Myocardium. *ACS nano*. 2019;13(9):9880-9894. doi:10.1021/acsnano.9b03343

41. Qin X, Chen H, Yang H, et al. Photoacoustic Imaging of Embryonic Stem Cell-Derived Cardiomyocytes in Living Hearts with Ultrasensitive Semiconducting Polymer Nanoparticles. *Adv Funct Mater*. Jan 4 2018;28(1)doi:10.1002/adfm.201704939

42. Sahoo S, Chung C, Khetan S, Burdick JA. Hydrolytically degradable hyaluronic acid hydrogels with controlled temporal structures. *Biomacromolecules*. Apr 2008;9(4):1088-92. doi:10.1021/bm800051m

43. Ouyang L, Highley CB, Rodell CB, Sun W, Burdick JA. 3D Printing of Shear-Thinning Hyaluronic Acid Hydrogels with Secondary Cross-Linking. *ACS Biomater Sci Eng*. Oct 10 2016;2(10):1743-1751. doi:10.1021/acsbiomaterials.6b00158

44. Hui E, Gimeno KI, Guan G, Caliari SR. Spatiotemporal Control of Viscoelasticity in Phototunable Hyaluronic Acid Hydrogels. *Biomacromolecules*. Nov 11 2019;20(11):4126-4134. doi:10.1021/acs.biomac.9b00965

45. Hahn SK, Park JK, Tomimatsu T, Shimoboji T. Synthesis and degradation test of hyaluronic acid hydrogels. *Int J Biol Macromol*. Mar 10 2007;40(4):374-80. doi:10.1016/j.ijbiomac.2006.09.019

46. Oh EJ, Kang SW, Kim BS, Jiang G, Cho IH, Hahn SK. Control of the molecular degradation of hyaluronic acid hydrogels for tissue augmentation. *J Biomed Mater Res A*. Sep 2008;86(3):685-93. doi:10.1002/jbm.a.31681

47. Hachet E, Van Den Berghe H, Bayma E, Block MR, Auzely-Velty R. Design of biomimetic cell-interactive substrates using hyaluronic acid hydrogels with tunable mechanical properties. *Biomacromolecules*. Jun 11 2012;13(6):1818-27. doi:10.1021/bm300324m

48. Imato K, Nishihara M, Kanehara T, Amamoto Y, Takahara A, Otsuka H. Self-healing of chemical gels cross-linked by diarylbibenzofuranone-based trigger-free dynamic covalent bonds at room temperature. *Angew Chem Int Ed Engl*. Jan 27 2012;51(5):1138-42. doi:10.1002/anie.201104069

49. Rodell CB, MacArthur JW, Dorsey SM, et al. Shear-Thinning Supramolecular Hydrogels with Secondary Autonomous Covalent Crosslinking to Modulate Viscoelastic Properties In Vivo. *Adv Funct Mater*. Jan 28 2015;25(4):636-644. doi:10.1002/adfm.201403550

50. Hafeez S, Ooi HW, Morgan FLC, et al. Viscoelastic Oxidized Alginates with Reversible Imine Type Crosslinks: Self-Healing, Injectable, and Bioprintable Hydrogels. *Gels*. Nov 21 2018;4(4)doi:10.3390/gels4040085

51. Kan HC, Ferry JD. Trapped Entanglements Vs Dissociable Junctions in Networks Cross-Linked in Strained States. *Macromolecules*. 1980;13(5):1313-1314. doi:DOI 10.1021/ma60077a054

52. Graessley WW. The entanglement concept in polymer rheology. Berlin ;: Springer-Verlag; 1974.

53. Mouser VH, Melchels FP, Visser J, Dhert WJ, Gawlitta D, Malda J. Yield stress determines bioprintability of hydrogels based on gelatin-methacryloyl and gellan gum for cartilage bioprinting. *Biofabrication*. Jul 19 2016;8(3):035003. doi:10.1088/1758-5090/8/3/035003

54. Jons CK, Grosskopf AK, Baillet J, et al. Yield-Stress and Creep Control Depot Formation and Persistence of Injectable Hydrogels Following Subcutaneous Administration. *Advanced Functional Materials*. 2022;32(40):2203402. doi:https://doi.org/10.1002/adfm.202203402

55. Yan C, Altunbas A, Yucel T, Nagarkar RP, Schneider JP, Pochan DJ. Injectable solid hydrogel: mechanism of shear-thinning and immediate recovery of injectable beta-

hairpin peptide hydrogels. *Soft Matter*. Oct 21 2010;6(20):5143-5156. doi:10.1039/C0SM00642D

56. Wu P, Feldman AK, Nugent AK, et al. Efficiency and fidelity in a click-chemistry route to triazole dendrimers by the copper(i)-catalyzed ligation of azides and alkynes. *Angew Chem Int Ed Engl*. Jul 26 2004;43(30):3928-32. doi:10.1002/anie.200454078

57. Rostovtsev VV, Green LG, Fokin VV, Sharpless KB. A stepwise huisgen cycloaddition process: copper(I)-catalyzed regioselective "ligation" of azides and terminal alkynes. *Angew Chem Int Ed Engl*. Jul 15 2002;41(14):2596-9. doi:10.1002/1521-3773(20020715)41:14<2596::AID-ANIE2596>3.0.CO;2-4

58. Anseth KS, Klok HA. Click Chemistry in Biomaterials, Nanomedicine, and Drug Delivery. *Biomacromolecules*. Jan 11 2016;17(1):1-3. doi:10.1021/acs.biomac.5b01660

59. Madl CM, Heilshorn SC. Bioorthogonal Strategies for Engineering Extracellular Matrices. *Adv Funct Mater*. Mar 14 2018;28(11)doi:10.1002/adfm.201706046

60. Madl CM, Katz LM, Heilshorn SC. Tuning Bulk Hydrogel Degradation by Simultaneous Control of Proteolytic Cleavage Kinetics and Hydrogel Network Architecture. *ACS Macro Lett*. Nov 20 2018;7(11):1302-1307. doi:10.1021/acsmacrolett.8b00664

61. McKinnon DD, Domaille DW, Cha JN, Anseth KS. Biophysically defined and cytocompatible covalently adaptable networks as viscoelastic 3D cell culture systems. *Adv Mater*. Feb 12 2014;26(6):865-72. doi:10.1002/adma.201303680

62. Shin M, Shin S-H, Lee M, et al. Rheological criteria for distinguishing self-healing and non-self-healing hydrogels. *Polymer*. 2021/08/16/ 2021;229:123969. doi:https://doi.org/10.1016/j.polymer.2021.123969

63. Cheng N, Zhang Y, Wu Y, et al. Hydrogel platform capable of molecularly resolved pulling on cells for mechanotransduction. *Mater Today Bio*. Dec 15 2022;17:100476. doi:10.1016/j.mtbio.2022.100476

64. Muir VG, Prendergast ME, Burdick JA. Fragmenting Bulk Hydrogels and Processing into Granular Hydrogels for Biomedical Applications. *J Vis Exp*. May 17 2022;(183)doi:10.3791/63867

65. Muir VG, Qazi TH, Weintraub S, Torres Maldonado BO, Arratia PE, Burdick JA. Sticking Together: Injectable Granular Hydrogels with Increased Functionality via Dynamic Covalent Inter-Particle Crosslinking. *Small*. Sep 2022;18(36):e2201115. doi:10.1002/smll.202201115

66. Chen H, Fei F, Li X, et al. A structure-supporting, self-healing, and high permeating hydrogel bioink for establishment of diverse homogeneous tissue-like

constructs. *Bioact Mater*. Oct 2021;6(10):3580-3595. doi:10.1016/j.bioactmat.2021.03.019

67. Krieghoff J, Rost J, Kohn-Polster C, et al. Extrusion-Printing of Multi-Channeled Two-Component Hydrogel Constructs from Gelatinous Peptides and Anhydride-Containing Oligomers. *Biomedicines*. Apr 1 2021;9(4)doi:10.3390/biomedicines9040370

68. Lee SC, Gillispie G, Prim P, Lee SJ. Physical and Chemical Factors Influencing the Printability of Hydrogel-based Extrusion Bioinks. *Chem Rev*. Oct 14 2020;120(19):10834-10886. doi:10.1021/acs.chemrev.0c00015

69. Larsen D, Kietrys AM, Clark SA, Park HS, Ekebergh A, Kool ET. Exceptionally rapid oxime and hydrazone formation promoted by catalytic amine buffers with low toxicity. *Chem Sci*. Jun 21 2018;9(23):5252-5259. doi:10.1039/c8sc01082j

70. Proksch E. pH in nature, humans and skin. *J Dermatol*. Sep 2018;45(9):1044-1052. doi:10.1111/1346-8138.14489

71. Ferry JD. Viscoelastic properties of polymers. New York: Wiley; 1961.

72. Zhong M, Wang R, Kawamoto K, Olsen BD, Johnson JA. Quantifying the impact of molecular defects on polymer network elasticity. *Science*. Sep 16 2016;353(6305):1264-8. doi:10.1126/science.aag0184

73. Queslel JP, Mark JE. Molecular Interpretation of the Moduli of Elastomeric Polymer Networks of Known Structure. *Adv Polym Sci*. 1984;65:135-176. doi:DOI 10.1007/BFb0017103

74. Winter HH, Chambon F. Analysis of Linear Viscoelasticity of a Crosslinking Polymer at the Gel Point. *J Rheol*. 1986;30(2):367-382. doi:10.1122/1.549853

75. Bonino CA, Samorezov JE, Jeon O, Alsberg E, Khan SA. Real-time in situ rheology of alginate hydrogel photocrosslinking. *Soft Matter*. 2011;7(24):11510. doi:10.1039/c1sm06109g

76. Zuidema JM, Rivet CJ, Gilbert RJ, Morrison FA. A protocol for rheological characterization of hydrogels for tissue engineering strategies. *Journal of Biomedical Materials Research Part B: Applied Biomaterials*. 2014;102(5):1063-1073. doi:10.1002/jbm.b.33088

77. Chambon F, Winter HH. Stopping of crosslinking reaction in a PDMS polymer at the gel point. *Polymer Bulletin*. 1985;13(6)doi:10.1007/bf00263470

78. Fletcher EE, Yan DD, Kosiba AA, Zhou Y, Shi HF. Biotechnological applications of elastin-like polypeptides and the inverse transition cycle in the pharmaceutical industry. *Protein Expres Purif*. Jan 2019;153:114-120. doi:10.1016/j.pep.2018.09.006

79. Wang H, Paul A, Nguyen D, Enejder A, Heilshorn SC. Tunable Control of Hydrogel Microstructure by Kinetic Competition between Self-Assembly and Crosslinking of Elastin-like Proteins. *ACS Applied Materials & Interfaces*. 2018;10(26):21808-21815. doi:10.1021/acsami.8b02461

80. Deforest CA, Sims EA, Anseth KS. Peptide-Functionalized Click Hydrogels with Independently Tunable Mechanics and Chemical Functionality for 3D Cell Culture. *Chemistry of Materials*. 2010;22(16):4783-4790. doi:10.1021/cm101391y

81. Kizilay MY, Okay O. Effect of hydrolysis on spatial inhomogeneity in poly (acrylamide) gels of various crosslink densities. *Polymer*. Aug 2003;44(18):5239-5250. doi:10.1016/S0032-3861(03)00494-4

82. Rebello NJ, Beech HK, Olsen BD. Adding the Effect of Topological Defects to the Flory–Rehner and Bray–Merrill Swelling Theories. *ACS Macro Letters*. 2021;10(5):531-537. doi:10.1021/acsmacrolett.0c00909

83. Vilgis TA, Heinrich G. The Essential Role of Network Topology in Rubber Elasticity. *Angew Makromol Chem*. Dec 1992;202:243-259. doi:DOI 10.1002/apmc.1992.052020114

84. Tobita H, Hamielec AE. Cross-Linking Kinetics in Polyacrylamide Networks. *Polymer*. Aug 1990;31(8):1546-1552. doi:Doi 10.1016/0032-3861(90)90163-S

85. Di Lorenzo F, Seiffert S. Nanostructural heterogeneity in polymer networks and gels. *Polymer Chemistry*. 2015;6(31):5515-5528. doi:10.1039/c4py01677g

86. De Gennes P-G, Gennes P-G. *Scaling concepts in polymer physics*. Cornell university press; 1979.

87. Stepto RFT, Cail JI, Taylor DJR. Predicting the formation, structure and elastomeric properties of end-linked polymer networks. *Macromolecular Symposia*. Oct 2000;159:163-178. doi:Doi 10.1002/1521-3900(200010)159:1<163::Aid-Masy163>3.0.Co;2-#

88. Flory PJ. *Principles of polymer chemistry*. The George Fisher Baker non-resident lectureship in chemistry at Cornell University. Cornell University Press; 1953:672 p.

89. Stockmayer WH. Theory of molecular size distribution and gel formation in branched polymers II General cross linking. *J Chem Phys*. Apr 1944;12(4):125-131. doi:Doi 10.1063/1.1723922

90. Stauffer D, Aharony A. *Introduction to percolation theory*. Rev., 2nd ed. Taylor & Francis; 1994:x, 181 p.

91. Leibler L, Rubinstein M, Colby RH. Dynamics of Reversible Networks. *Macromolecules*. Aug 5 1991;24(16):4701-4707. doi:DOI 10.1021/ma00016a034

92. Rubinstein M, Semenov AN. Dynamics of entangled solutions of associating polymers. *Macromolecules*. Feb 13 2001;34(4):1058-1068. doi:10.1021/ma0013049

93. Chen Q, Tudryn GJ, Colby RH. Ionomer dynamics and the sticky Rouse model. *J Rheol*. Sep 2013;57(5):1441-1462. doi:10.1122/1.4818868

94. Tang S, Wang M, Olsen BD. Anomalous self-diffusion and sticky Rouse dynamics in associative protein hydrogels. *J Am Chem Soc*. Mar 25 2015;137(11):3946-57. doi:10.1021/jacs.5b00722

95. Cai PC, Krajina BA, Spakowitz AJ. Brachiation of a polymer chain in the presence of a dynamic network. *Physical Review E*. 2020;102(2)doi:10.1103/physreve.102.020501

96. Cai PC, Su B, Zou L, Webber MJ, Heilshorn SC, Spakowitz AJ. Rheological Characterization and Theoretical Modeling Establish Molecular Design Rules for Tailored Dynamically Associating Polymers. *ACS Central Science*. 2022;8(9):1318-1327. doi:10.1021/acscentsci.2c00432

97. Lang M, Kreitmeier S, Goritz D. Trapped entanglements in polymer networks. *Rubber Chem Technol*. Nov-Dec 2007;80(5):873-894. doi:Doi 10.5254/1.3539422

98. Van Durme K, Rahier H, Van Mele B. Influence of additives on the thermoresponsive behavior of polymers in aqueous solution. *Macromolecules*. Nov 29 2005;38(24):10155-10163. doi:10.1021/ma051816t

99. Reguera J, Urry DW, Parker TM, McPherson DT, Rodriguez-Cabello JC. Effect of NaCl on the exothermic and endothermic components of the inverse temperature transition of a model elastin-like polymer. *Biomacromolecules*. Feb 2007;8(2):354-8. doi:10.1021/bm060936l

100. Balu R, Whittaker J, Dutta NK, Elvin CM, Choudhury NR. Multi-responsive biomaterials and nanobioconjugates from resilin-like protein polymers. *J Mater Chem B*. Sep 28 2014;2(36):5936-5947. doi:10.1039/c4tb00726c

101. Ono Y, Shikata T. Hydration and dynamic behavior of poly(N-isopropylacrylamide)s in aqueous solution: A sharp phase transition at the lower critical solution temperature. *Journal of the American Chemical Society*. Aug 9 2006;128(31):10030-10031. doi:ARTN JA063990I

10.1021/ja063990i

102. Oelschlaeger C, Cota Pinto Coelho M, Willenbacher N. Chain Flexibility and Dynamics of Polysaccharide Hyaluronan in Entangled Solutions: A High Frequency Rheology and Diffusing Wave Spectroscopy Study. *Biomacromolecules*. 2013;14(10):3689-3696. doi:10.1021/bm4010436

103. Lopez Hernandez H, Souza JW, Appel EA. A Quantitative Description for Designing the Extrudability of Shear-Thinning Physical Hydrogels. *Macromol Biosci*. Feb 2021;21(2):e2000295. doi:10.1002/mabi.202000295

104. Guvendiren M, Lu HD, Burdick JA. Shear-thinning hydrogels for biomedical applications. *Soft Matter*. 2012;8(2):260-272. doi:10.1039/c1sm06513k

05. Olsen BD, Kornfield JA, Tirrell DA. Yielding Behavior in Injectable Hydrogels from Telechelic Proteins. *Macromolecules*. Nov 9 2010;43(21):9094-9099. doi:10.1021/ma101434a

106. Bertsch P, Diba M, Mooney DJ, Leeuwenburgh SCG. Self-Healing Injectable Hydrogels for Tissue Regeneration. *Chemical Reviews*. Jan 25 2023;123(2):834-873. doi:10.1021/acs.chemrev.2c00179

107. Lee HP, Deo KA, Jeong J, et al. Injectable, Self-healing, and 3D Printable Dynamic Hydrogels. *Advanced Materials Interfaces*. 2022;9(23):2201186. doi:10.1002/admi.202201186

108. Lou J, Liu F, Lindsay CD, Chaudhuri O, Heilshorn SC, Xia Y. Dynamic Hyaluronan Hydrogels with Temporally Modulated High Injectability and Stability Using a Biocompatible Catalyst. *Advanced Materials*. 2018;30(22):1705215. doi:10.1002/adma.201705215

109. Zhu DQ, Wang HY, Trinh P, Heilshorn SC, Yang F. Elastin-like protein-hyaluronic acid (ELP-HA) hydrogels with decoupled mechanical and biochemical cues for cartilage regeneration. *Biomaterials*. May 2017;127:132-140. doi:10.1016/j.biomaterials.2017.02.010

110. Schneider JP, Pochan DJ, Ozbas B, Rajagopal K, Pakstis L, Kretsinger J. Responsive hydrogels from the intramolecular folding and self-assembly of a designed peptide. *J Am Chem Soc*. Dec 18 2002;124(50):15030-7. doi:10.1021/ja027993g

111. Dinkgreve M, Paredes J, Denn MM, Bonn D. On different ways of measuring "the" yield stress. *J Non-Newton Fluid*. Dec 2016;238:233-241. doi:10.1016/j.jnnfm.2016.11.001

112. Nguyen QD, Boger DV. Measuring the Flow Properties of Yield Stress Fluids. *Annu Rev Fluid Mech*. 1992;24:47-88. doi:DOI 10.1146/annurev.fl.24.010192.000403

113. Garcia MC, Alfaro MC, Munoz J. Creep-recovery-creep tests to determine the yield stress of fluid gels containing gellan gum and Na+. *Biochem Eng J*. Oct 15 2016;114:260-264. doi:10.1016/j.bej.2016.07.010

114. Robinson TE, Hughes EAB, Bose A, et al. Filling the Gap: A Correlation between Objective and Subjective Measures of Injectability. *Adv Healthc Mater*. Mar 2020;9(5):e1901521. doi:10.1002/adhm.201901521

115. Luo Y, Kobler JB, Heaton JT, Jia X, Zeitels SM, Langer R. Injectable hyaluronic acid-dextran hydrogels and effects of implantation in ferret vocal fold. *J Biomed Mater Res B Appl Biomater*. May 2010;93(2):386-93. doi:10.1002/jbm.b.31593

116. Uman S, Dhand A, Burdick JA. Recent advances in shear-thinning and self-healing hydrogels for biomedical applications. *Journal of Applied Polymer Science*. 2020;137(25):48668. doi:10.1002/app.48668

117. Bhattacharjee M, Escobar Ivirico JL, Kan H-M, et al. Injectable amnion hydrogel-mediated delivery of adipose-derived stem cells for osteoarthritis treatment. *Proceedings of the National Academy of Sciences*. 2022;119(4):e2120968119. doi:10.1073/pnas.2120968119

118. Aguado BA, Mulyasasmita W, Su J, Lampe KJ, Heilshorn SC. Improving viability of stem cells during syringe needle flow through the design of hydrogel cell carriers. *Tissue Eng Part A*. Apr 2012;18(7-8):806-15. doi:10.1089/ten.TEA.2011.0391

119. Chilton RA, Stainsby R. Pressure loss equations for laminar and turbulent non-Newtonian pipe flow. *J Hydraul Eng-Asce*. May 1998;124(5):522-529. doi:Doi 10.1061/(Asce)0733-9429(1998)124:5(522)

120. Bilgin C, Hutar J, Li JH, Castano O, Ribo M, Kallmes DF. Catheter design primer for neurointerventionalists. *J Neurointerv Surg*. Dec 7 2022;doi:10.1136/jnis-2022-019567

121. Chen MH, Wang LL, Chung JJ, Kim YH, Atluri P, Burdick JA. Methods To Assess Shear-Thinning Hydrogels for Application As Injectable Biomaterials. *Acs Biomaterials Science & Engineering*. Dec 2017;3(12):3146-3160. doi:10.1021/acsbiomaterials.7b00734

122. Sisso AM, Boit MO, DeForest CA. Self-healing injectable gelatin hydrogels for localized therapeutic cell delivery. *Journal of Biomedical Materials Research Part A*. May 2020;108(5):1112-1121. doi:10.1002/jbm.a.36886

123. Nelson BR, Kirkpatrick BE, Miksch CE, et al. Photoinduced Dithiolane Crosslinking for Multiresponsive Dynamic Hydrogels. *Advanced Materials*. Mar 11 2023;doi:10.1002/adma.202211209

124. Gaharwar AK, Avery RK, Assmann A, et al. Shear-thinning nanocomposite hydrogels for the treatment of hemorrhage. *ACS nano*. Oct 28 2014;8(10):9833-42. doi:10.1021/nn503719n

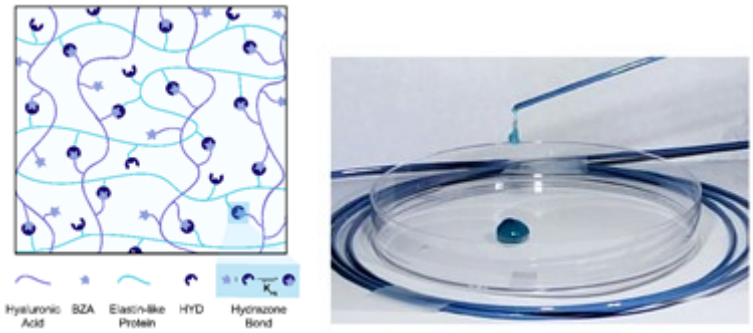

Dynamic covalent chemistry (**DCC**) crosslinks can form hydrogels with tunable mechanical properties permissive to injectability and self-healing. However, not all hydrogels with transient crosslinks are easily extrudable. This work highlights the importance of polymer molecular weight and crosslinking functionality in influencing the injectability and network formation of DCC-crosslinked hydrogels and aims to guide future design of injectable hydrogels.